Summer 2017

α-Eleostearic Acid Extraction by Saponification of Tung Oil and Its Subsequent Polymerization

Amanda Murawski

α-ELEOSTEARIC ACID EXTRACTION BY SAPONIFICATION OF TUNG OIL AND ITS SUBSEQUENT POLYMERIZATION

by

AMANDA MURAWSKI

(Under the Direction of Rafael L. Quirino)

ABSTRACT

The goal of environmentally sound research is to provide alternatives that are more sustainable and renewable, such as vegetable oil-based polymers, than the current petroleum-based products. Vegetable oil-based polymers have received a lot of attention recently due their multifaceted properties, which are simply achieved by adjusting the monomer or resin composition. The carbon-carbon double bonds in unsaturated oils are ideal reactive sites for the free radical or cationic polymerizations. Most vegetable oils must be modified before polymerization due to the low reactivity of their non-conjugated fatty acid chains. Tung oil (TO) contains ~83% of a triply conjugated fatty acid (α-eleostearic acid), making it an attractive starting material. Without the reinforcing role of fibers, such as cellulose, vegetable oil-based polymers do not have the thermo-mechanical properties to replace petroleum-based polymers. Compatibilizers, such as asolectin and maleic anhydride, have been utilized to enhance the adhesion between resin and reinforcement, consequently enhancing the composites' thermo-mechanical properties. In this manuscript, the need for a compatibilizer is eliminated through the preparation of a polar matrix from the crosslinking of tung oil fatty acids with the co-monomers divinylbenzene and *n*-butyl methacrylate. It is shown that the polar regions of the fatty acid can interact directly with a polar reinforcement, such as α-cellulose, through hydrogen bonding. The successful isolation of fatty acids from tung oil was verified by GC-MS, ^{1}H NMR, Raman, and FT-IR spectroscopies. The

optimal cure schedule was determined by DSC and DEA. The thermo-mechanical properties were analyzed by TGA, DSC, and DMA.

KEYWORDS: Bio-based materials, Renewable polymers, Thermosets, Tung oil, Free radical polymerization, Cellulose composites.

α-ELEOSTEARIC ACID EXTRACTION BY SAPONIFICATION OF TUNG OIL AND ITS SUBSEQUENT POLYMERIZATION

by

AMANDA MURAWSKI

B.S., Georgia Southern University, 2015

A Thesis Submitted to the Graduate Faculty of Georgia Southern University in

Partial Fulfillment of the Requirements for the Degree

MASTER OF SCIENCE

STATESBORO, GEORGIA

α-ELEOSTEARIC ACID EXTRACTION BY SAPONIFICATION OF TUNG OIL AND ITS SUBSEQUENT POLYMERIZATION

by

AMANDA MURAWSKI

Major Professor: Rafael L. Quirino

Committee: Christine Whitlock

Mujibur Khan

Electronic Version Approved:

July 2017

DEDICATION

To my Granna, my biggest supporter, and whom will forever be missed.

ACKNOWLEDGEMENTS

I would like to formally thank and would like to express my sincere gratitude to Herty Advanced Materials Development Center at Georgia Southern University and Georgia Southern University's Department of Chemistry and Biochemistry for their financial support for research and travel.

I want to thank my thesis committee members, Dr. Christine Whitlock, and Dr. Mujibur Khan, for their expertise, valuable time, and insightful comments. Additionally, I would like to thank the Applied Physical Science program within the Department of Chemistry and Biochemistry at Georgia Southern University for allowing the use of their facilities, graduate tuition waiver and graduate assistant funding. Dr. Weihua Ming and his research group for their assistance and guidance with contact angle goniometer. Dr. McGibony for her support and guidance as the Applied Physical Science graduate program director. Dr. Hao Chen for his guidance with SEM. Dr. Nathan Takas for his continuous patience and assistance with numerous instruments. The Quirino research group and fellow graduate students for their support and encouragement.

I would like to especially thank my research advisor, Dr. Rafael L. Quirino for his continuous patience, immense knowledge and support throughout the program. He is truly a great advisor and I would not have developed into the researcher I am today without his help. Lastly, I need to thank my family and friends for keeping me sane throughout the past two years.

TABLE OF CONTENTS

LIST OF TABLES

LIST OF FIGURES

THESIS ORGANIZATION

This thesis is separated into five chapters. Chapter 1 introduces the environmental importance of bio-based materials and presents a literature review of past research regarding the applications of vegetable oil based polymers. Chapter 1 ends with a central focus on tung oil derived polymers and the current manuscript's objectives. Chapter 2 expands on the experimental methods of the fatty acid extraction and isolation from tung oil. Chapter 2 ends with the analytical characterization of the extracted fatty acid, α-eleostearic acid. As well as a detailed synthesis description of one of the reference materials, methyl ester of α-eleostearic acid. Chapter 3 explains the free radical polymerization mechanism, and analytical characterization of the newly formed resins. Chapter 4 goes on to discuss the addition of cellulose as a reinforcement, and the subsequent composite characterization. Lastly, the general conclusions from the research are discussed in Chapter 5, along with the plans for future research.

CHAPTER 1: INTRODUCTION

Bio-based polymers utilize starting materials that are generally more sustainable and renewable than the current market's materials. Such products include vegetable oil based polymers. These polymers have received a lot of attention in research due to their versatility and tunable properties, which can be easily achieved by adjusting the resin composition. Some applications for these materials include research areas in biofuels, biomedical, adhesives and coatings. It is fundamentally accepted in the scientific community that fossil fuels are limited and nonrenewable.[1] Even so, there is an ongoing debate regarding the timeframe of when fossil fuels will be depleted. It is easy to forget the importance of bio-based research, since petroleum prices have leveled off from their economical peak. Although the current prices of petroleum are low, it is imperative and relative to continue research for bio-based alternatives to mitigate economical losses with the frequent fluctuations in petroleum price. Research has shown that the price of oil is not linearly correlated with the resource availability.[2] On top of lowering petroleum depletion impacts, it is important to introduce alternatives for environmental reasons and hazardous waste disposal concerns. Originally, vegetable oil based polymers were deemed too expense for practical applications. Through the advancement of technology, in addition to the low cost and ease of processability of non-edible oils like tung oil, manufacturing costs have been alleviated.[1,3]

Outside the realm of biofuels and drying agents, vegetable oils are important in food, cosmetics, soap production, detergents, and pharmaceuticals.[4] Tung oil and other vegetable oils are made up of triglyceride units, which are glycerol esters connected to unsaturated or saturated fatty acid chains ranging from 8 to 24 carbons (Figure 1). The compositions of the fatty chains are highly dependent on the plant type, agriculture conditions, and plant geography. Even oils extracted from the same plant, but from different locations within the plant, are subject to have

differing compositions of fatty acid chains;[5,6] yielding a wide range of potential properties in a singular plant. The carbon-carbon double bonds (C-C) in the unsaturated fatty acid chains give rise to ideal reactive sites for the chemical industry.[7] Chemical modification constructed at these unsaturated sites within the fatty acid chains have been widely studied for the production of polymeric materials. To further expand on the versatile processability of vegetable oil based polymers, two other novel polymerization methods should be noted. In one method, the triglycerides of vegetable oils are reduced via glycerolysis to their monoglyceride, diglyceride, and glycerol units. Then is reacted with maleic anhydride to produce a mixture of monoglycerides, diglycerides, and glycerol maleate half esters. These maleate half esters are relatively unreactive towards one another, therefore, co-monomers such as styrene (ST), are introduced into the polymerization reaction to increase reactivity. In the other method, the unsaturated regions of the fatty acid chain were functionalized first, then respective the monoglycerides or diglycerides were extracted.[8] These newly functionalized moieties, generally containing mostly epoxy or hydroxyl groups, can be further used in radical, cationic, polycondensation, ring-opening, thermal, and other polymerization reactions.[9,10,11]

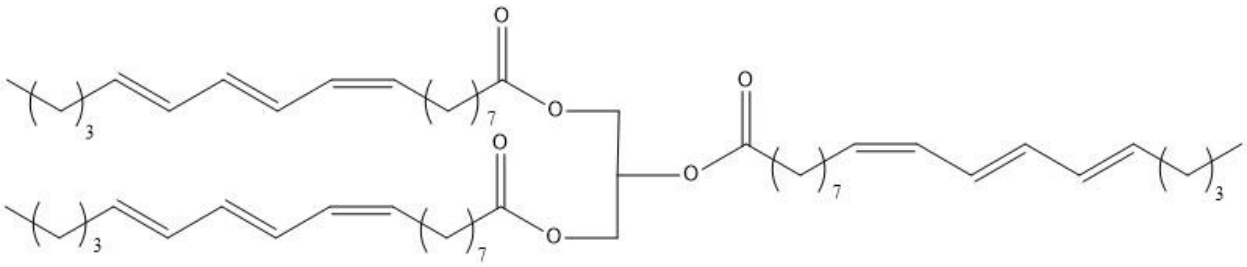

Figure 1. Triglyceride structure of Tung oil represented with its' fatty chain α-eleostearic acid (C18:3). Tung oil also contains ~15% oleic acid (C18:1), ~1% palmitic acid (C18:0) and ~1% stearic acid (C16:0). Adapted from Schönemann et al. (2006).[12]

Polymers can be divided up into two categories: thermosets or thermoplastics. Thermoplastics are held together by compact, non-covalent interactions which can be melted down and recycled at the end of the polymer's life cycle. On the other hand, thermosets consist of monomer chains that are covalently cross-linked, resulting in a rigid, interconnected structure. Thermosets do not melt and can not be dissolved in a solvent. Consequently, thermosets must undergo harsher conditions to be recycled due to their enhanced mechanical properties compared to thermoplastics. Currently, majority of thermosetting polymeric materials are derived from petroleum based materials and are non-biodegradable.[13,14] Development of new thermosetting polymers that are derived from renewable feedstocks are not only novel and environmentally friendly, but economically beneficious as well. Generally, thermosets and thermoplastics derived from vegetable oils exhibit flexible, long-chain polymer characteristics such as high elongation at break, low glass transition temperatures, and relatively low stiffness.[15] Reasonably, it is not common to use a pure bio-resins as part of a composite. To enhance the rigidity and increase the glass transition temperature, polymer blends of synthetic and renewable resins are used.

As previously mentioned, most oils must be modified before polymerization due to the low reactivity of their non-conjugated fatty acid chains. Tung oil has approximately 83% of its fatty acid chains composing of α-eleostearic acid, a naturally triply conjugated fatty acid, and does not have to be functionalized to undergo polymerization. The Carbon–Carbon double bonds in tung oil (at carbons 9 cis, 11 trans, 13 trans)[16] can readily react and polymerize in the presence of oxygen,[17] as well as with vinyl or acrylic co-monomers via cationic, thermal, or free radical polymerizations, resulting in rigid, crosslinked polymers.[18] The auto-oxidative behavior of tung oil is quite unique and has been the central focus in several research studies. Meiorin et al. (2013) found an enhancement of mechanical properties in 2 year-old aged samples in reference

to freshly cured samples. Different compositions of tung oil, divinylbenzene, and styrene were polymerized via cationic polymerization and their respective polymers studied.[19] One of the limitations of utilizing olefins for polymerization reactions is that not all the double bonds are completely reacted even though the polymerization has gone to completion. The unreacted double-bonds are generally a source of degradation or chain scission and have negative impacts on the mechanical properties. But in some oils, like linseed and tung oil, the unreacted oil chains can act as plasticizers, and once exposed to air, the unreacted double bonds will oxidize and become incorporated into the polymeric network, therefore, enhancing the mechanical properties.[20] Besides linolenic acid, α-eleostearic acid is the only other fatty acid that is commonly used in polymer chemistry that contains three C-C double bonds within its structure (Figure 2). Although, unlike linolenic acid, the three C-C double bonds in α-eleostearic acid are conjugated, giving tung oil an enhancement in reactivity. The alkene conjugation and the increase in reactivity is what makes tung oil such a great drying oil. The unsaturated chain reactivity has also been utilized in producing crosslinked thermosetting polymers co-polymerized divinylbenzene and styrene (ST).[21,22] Other studies have further shown that a biopolymer can successfully be prepared from tung oil by cationic polymerization with an application as a self-healing agent for the curing of microcracks.[23]

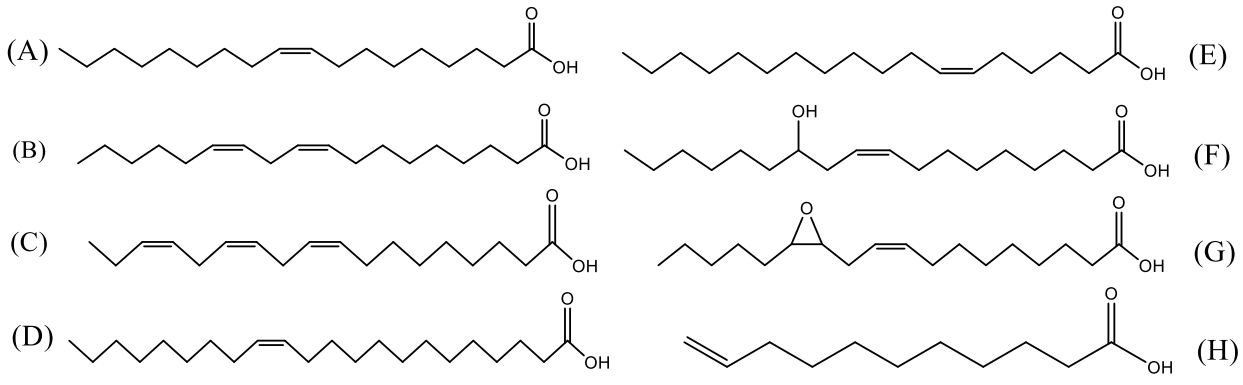

Figure 2. Frequently used fatty acids in polymer chemistry. (A) oleic acid, (B) linoleic acid, (C)

linolenic acid, (iv) erucic acid, (v) petroselinic acid, (vi) ricinoleic acid, (vii) vernolic acid, (viii) 10-undecenoic acid. Adapted from Montero de Espinosa and Meier (2011).[24]

Other environmentally alternative research has capitalized on the oils' promising results and ventured into the development of numerous bio-based resin systems. Polyurethanes,[25,26] polyester amides,[27] polyolefins,[28] and alkyd[29] resins are just some of the current resins on the market. In the case of alkyd resins used for coating applications, the binder (resin) can be viscous and therefore difficult to process. To overcome this viscosity problem, the respective resins are dissolved in volatile organic solvents (VOC) that lead to greenhouse gases.[29] Considering the current environmental concerns, it has become favored to use water-borne alkyd, polyurethane, epoxy, or acrylic resins due to their low or lack of VOC emissions released during polymer processing. Another recent development in efforts to decrease VOC emissions in coatings is to introduce a reactive diluent, tung oil, with the alkyd binder to decrease the initial viscosity without the use of an organic solvent.[30] Polyurethanes from modified tung oil have been studied. Tung oil was subjected to hydroxylation of the olefins in the fatty acid chains followed by alcoholysis with triethanolamine resulting in a high hydroxyl value of the newly obtained polyol. The modified tung oil polyol was reinforced with wood flour and microcrystalline cellulose, with the wood flour composite producing the best thermomechanical properties due to its better dispersion throughout the resin.[31]

Alone, bio-based resins do not have the mechanical properties to compete with the current petroleum based resins. Therefore, in addition with using polymer bends, synthetic fibers such as glass and nanoclays, have been used as reinforcements in these resins.[32,33] The difficulty with binding between polymer and reinforcement lies within the incompatibility between hydrophobic resin and the hydrophilic filler. A common solution to alleviate the incompatibility between resin

and filler, is to functionalize the reinforcing materials' surface,[34] as well as the use of more polar triglyceride derivatives for compatibility solutions. With the political and social push for more renewable and natural biocomposites, there has been a shift in research from synthetic fiber reinforcements to natural fibers and fillers. One potential problem with using bio friendly alternatives is the effect moisture has on the mechanical properties. As discovered in Mosiewicki et al. (2012) study, moisture exposure decreased the mechanical properties of tung oil based composites. Although, this decrease is not necessarily a negative aspect with respect to concerns of biodegradability and recyclability. Other studies have discovered that mixing tung oil, a viscous material, with other oils such as soybean oil, decreased the viscosity in the blended oil mixture and enhanced the processability.[17] Mechanical property improvements have been made at the reinforcement and resin interactions for by adding malic anhydride as a co-polymer to thermosets reinforced with rice hulls,[35] and wood flour.[36] Compatibilizers with hydrophobic and hydrophilic regions are a common solution to the resin-reinforcement incompatibility issue. Johns et al. (2015) found that asolectin, which has been previously used as a synthetic protein transport vessel,[37,38] due to its hydrophobicity nature of the carbon chains and hydrophilicity of the phosphate and ester heads, contains compatibilizer properties. This study found an enhancement of thermo-mechanical properties with the addition of the compatibilizer, asolectin, in tung oil/cellulose composites.[39]

Recently, much work on bio-based composites with natural fibers and fillers has been reported. Wool et al. (2006) prepared thermosets by modifying soybean and castor oils with maleic anhydride and copolymerizing with ST.[40] While other researchers have converted the internal C=C bonds of soybean oil into polyols to be reacted with isocyanates for the final production of polyurethane thermosets.[41,42] Often, there are large differences in reactivity between vegetable oils and their cross-linker co-monomers, ultimately resulting in oil-rich and oil-poor phases. In

vegetable oil-based polymers used in cationic polymerization with divinylbenzene (DVB), Norway fish oil (NFO) has been used to modify the cationic initiator-catalyst system to produce homogenous co-polymers due to its inherent ability to interact with DVB and vegetable oils.[43] Xia et al. (2008) found that thermosets prepared by cationic polymerization of Dilulin or ML189 and dicyclopentadiene (DCPD) with a boron trifluoride diethyl etherate (BFE) catalyst as the initiator, produced homogenous co-polymers. Since all monomers utilized in this polymerization displayed similar reactivity in relation to one another, the use of NFO as an initiator modifier was not needed.[44] Our group has successfully polymerized a variety of bio-based resins via cationic (Figure 3) and free radical (Figure 4) polymerizations utilizing the reactive internal olefins of tung oil,[39,45,46] and other vegetable oils for the production of polyurethanes,[47] and other biocomposites.[48] Some applications for these polymers include biofuels, construction, aerospace, and polyurethane based foams. Lignin is a naturally occurring polymer found in plants serving as a structural binder in the cell wall. Gibbons et al. (2015) co-polymerized modified lignin with *n*-butyl methacrylate (BMA), ST or DVB and found that the mechanical properties yielded results comparable to the commercially available Novolac Epoxy Resins® from Dow Plastics.[48] Smith et al. (2015) found that through the addition of carbon nanotubes (CNT) to the polymer resin, the cure time is significantly reduced when cured in the microwave. Although, with the reduced cure time, the mechanical properties were compromised in comparison with the same composition of resin and CNT cured in a programmable oven. Uniquely, the thermal properties of resins cured in the oven are independent of the CNT wt% while the resins cured in the microwave show an enhancement of thermal properties as CNT wt% increases.[46]

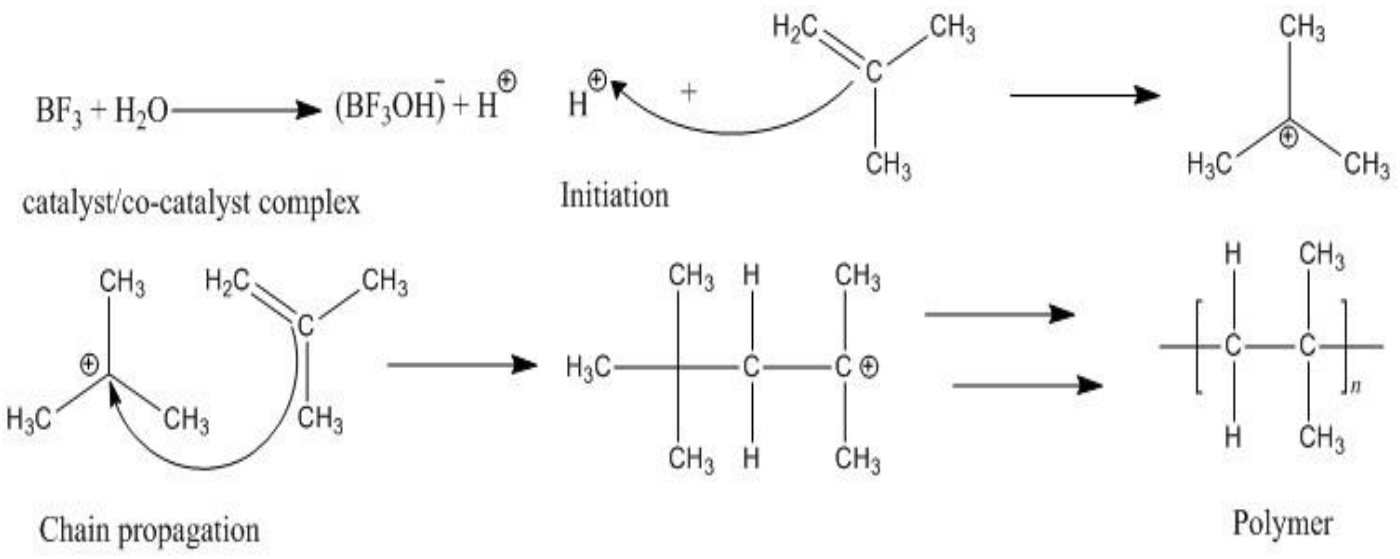

Figure 3. General cationic polymerization reaction mechanism. Adapted from Young and Lovell (2011).[49]

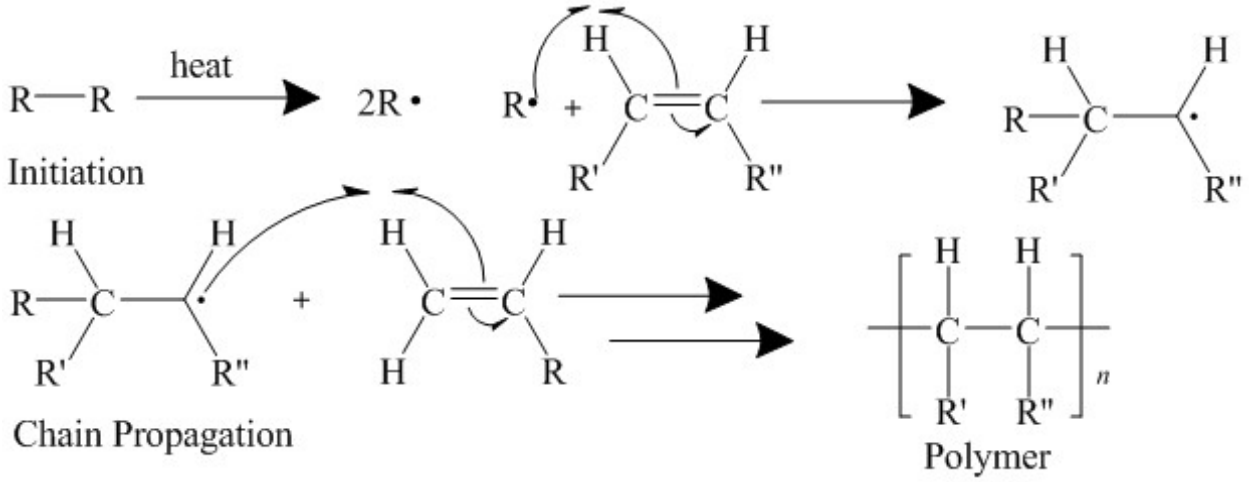

Figure 4. General free radical polymerization reaction mechanism. Adapted from Young and Lovell (2011).[49]

Based off the wide range of applications and versatility of tung oil monomers as shown from other polymer studies, it was time to take the previous research a step further. Cellulose is a hydrophilic polysaccharide, composed of repeating ß(1-4) linked D-glucose units[50] (Figure 5). Due to celluloses' biodegradability, accessibility, and mechanical properties it has become increasingly

popular for the production of low cost materials. Lignocellulosic and vegetable fibers have also been used as reinforcement in composites to improve mechanical properties and lower cost. In polyurethanes composites, the surface hydroxyl groups on cellulose can hydrogen bond with the resin's urethane groups to create an intermolecular connection between the two molecules.[25,51,52] The same principle can be applied to the current research. This manuscript aims to eliminate the need of a compatibilizer between the hydrophilic cellulose and hydrophobic tung oil. By extracting the fatty acid, *α*-eleostearic acid, from the glycerol motif of tung oil (Figure 6), a polymeric network containing hydroxyl groups with potential to hydrogen bond with polar reinforcements, such as cellulose, can be obtained. It is hypothesized that the polar groups within the tung oil fatty acid and cellulose can form a strong intermolecular hydrogen bonding network, therefore enhancing the thermo-mechanical properties. The successful isolation of fatty acids was checked by GC-MS, ^{1}H NMR, Raman, and FT-IR. The polymerization of the resins was monitored by dielectric analysis (DEA) and then analyzed by differential scanning calorimetry (DSC) for verification of cure completion. The resin and composite properties were tested with thermogravimetric analysis (TGA), dynamic mechanical analysis (DMA), contact angle goniometer, and scanning electron microscopy (SEM). Similar methyl esters of *α*-eleostearic acid, and tung oil resins and composites were analyzed under the same parameters listed above. A comparison study was conducted of the thermo-mechanical properties between the different composites.

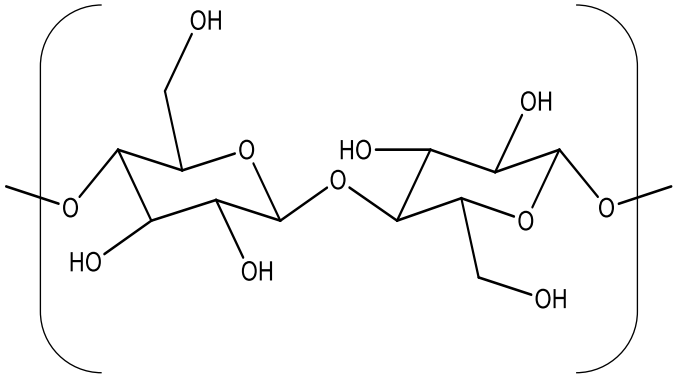

Figure 5. *α*-cellulose with ß(1-4) linked D-glucose monomer units. Adapted from Johns et al. (2015).

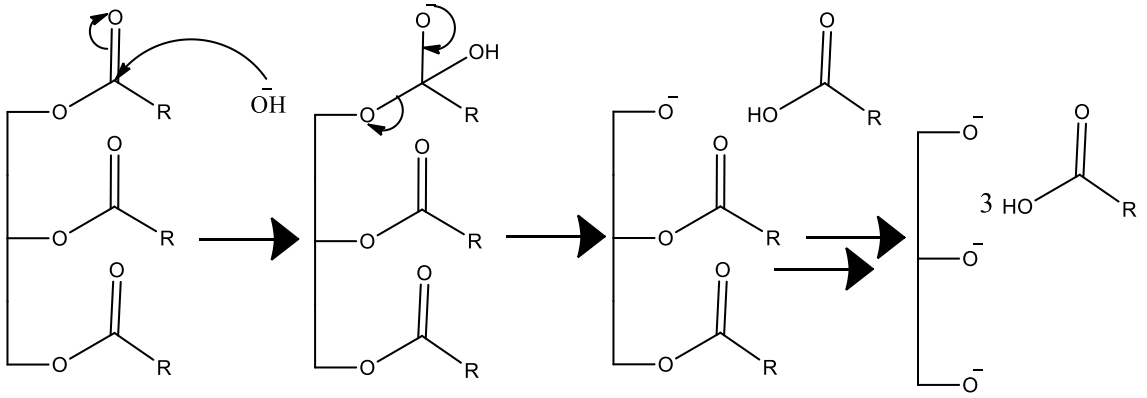

Figure 6. Saponification reaction under basic conditions (NaOH) with tung oil; separating the fatty acid chains from the glycerol backbone.

CHAPTER 2: FATTY ACID EXTRACTION AND ISOLATION

Fatty acid based polymers are commonly used in pharmaceuticals,[53] biofuels,[54] coatings and paints[55] for a series of different applications. Naturally, fatty acid monomers must undergo functionalization before polymerization due to their low reactivity of the internal unsaturated regions in the fatty acid chains. With the enhancement in reactivity due to the olefin conjugation in α-eleostearic acid's fatty acid chain, a subsequent polymer can be directly polymerized without prior functionalization. Tung oil contains approximately 83% of α-eleostearic acid in its fatty acid chains, making it can ideal candidate for extraction. Also, tung oil is a non-eligible vegetable oil, therefore the synthesis of materials derived from tung oil and its derivatives are not depleting food sources. A topic which has become a political and ethical concern regarding the usage of vegetable oils and their derivatives in polymer chemistry.

2.1 MATERIALS

The materials used in this section are tung oil (TO) (Sigma-Aldrich, St. Louis, MO), methanol, acetone (BDH Analytical Chemicals, Radnor, PA), 50% w/w sodium hydroxide solution (NaOH), hydrochloric acid (HCl), chloroform (Fisher Chemical, Fair Lawn, NJ), and deuterated chloroform (chloroform-D) (Cambridge Isotope Laboratories, Inc., Andover, MA). Gas-chromatography analyses were completed on a Shimadzu GC-17A Gas Chromatograph (GC) GCMS-QP5050A (Kyoto, Japan). The proton nuclear magnetic resonance (^{1}H-NMR) spectra were obtained on an Agilent MR400DD2 spectrometer (Santa Clara, CA) operating at 400 MHz. The raman spectrometry (Raman) studies were analyzed on a DXR Raman Microscope (Thermo Scientific, Waltham, MA) at a laser power of 1 mW.

2.2 FATTY ACID EXTRACTION BY SAPONIFICATION

Tung oil is naturally occurring vegetable oil composed of triglycerides containing three fatty acid chains and a glycerol backbone. Carboxylic acids are naturally more hydrophilic than ester groups. Additionally, the glycerol backbone provides rigidity and steric hindrance in comparison to free fatty acid chains. These components gave rise to the current research's objective of enhancing the resin-reinforcement interface by producing a more hydrophilic monomer; allowing the hydrophilic regions in the resin polymer and the hydrophilic regions in the reinforcement, cellulose, to favorably interact and hydrogen bond. Saponification reactions have been used for years, are well discussed in literature, and commonly used for the preparation of soap. Chemically speaking, a saponification reaction is the hydrolysis of esters in the presence of an alkaline compound.[56] The saponification reaction used for this manuscript was run under mild conditions and does not produce any harmful waste products.

The methodology used in this manuscript is a modified version of Hondred et al. (2014). First, 50% w/w sodium hydroxide solution (NaOH) was diluted to 20% w/w NaOH solution. Followed by an addition of 200 mL of the 20% sodium hydroxide (NaOH) solution per every 100 g of tung oil. The two reactants were mixed in a water bath under agitation with a magnetic stir bar at 70°C for 1 hour. Next, 300 mL of hot water was added to the solution and left to react for another 30 minutes. An additional 300 mL of hot water was added to the solution. Then 95 mL of hydrochloric acid was added to solution. The solution was left under heat and agitation for 1 hour. The fatty acid formed a precipitate. The newly formed precipitate was filtered and washed with 200 mL of water and 300 mL of methanol. The final product was dried under vacuum.

The hydrolysis of tung oil occurs is a multistep mechanism. First the hydroxide nucleophile generated from NaOH attacks at the electrophilic carbonyl carbon, breaking the π bond, pushing

the electron pair onto the oxygen. Therefore, creating a tetrahedral intermediate. Once the intermediate collapses, reforming the π bond between carbon and oxygen, the bond between the fatty acyl group carbon and the oxygen of the glycerol backbone break irreversibly. The freshly formed alkoxide creates a rapid acid-base reaction and deprotonates the fatty acid. HCl is added to neutralize the carboxylate; resulting in glycerol and 3 fatty acid chains (Figure 7).

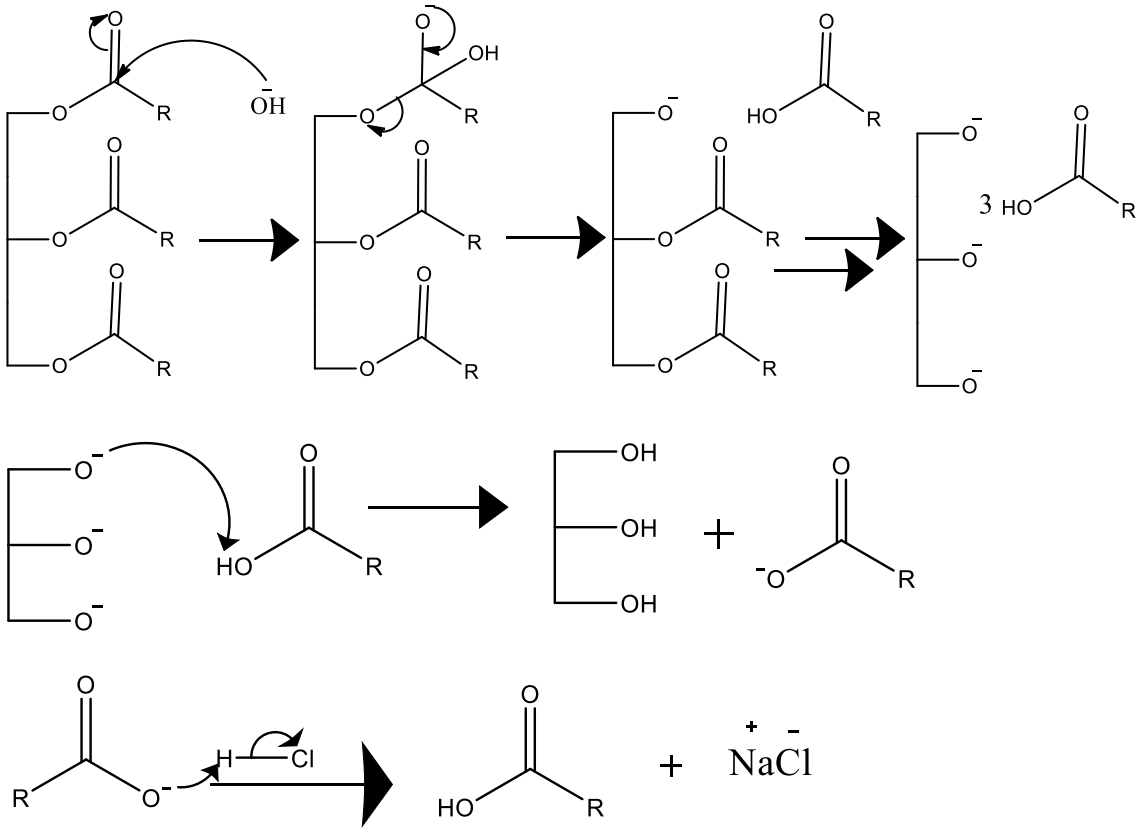

Figure 7. Reaction scheme of the extraction of *α*-eleostearic acid under basic conditions, and the acidification of the carboxylate ion.

2.3 METHYL ESTER SYNTHESIS BY TRANSESTERIFICATION

For comparison studies, methyl esters of tung oil were synthesized. A modified methodology for the methyl ester transesterification reaction[57] was adopted from Quirino et al. (2011). Initially, 20 g of pre-heated tung oil was reacted with 30 mL of methanol in a water bath.

The reaction was run under reflux and agitation by a magnetic stir bar at 55°C for 2 hours. Next, 0.5 g of 50% sodium hydroxide solution was used to catalyze the start of the reaction. Then, 100 mL of chloroform was added to the solution and mixed in a separatory funnel to separate glycerol from the newly formed methyl ester. After phase separation, the clear, bottom layer was decanted and the top layer with the methyl esters was analyzed for purity and successful isolation.

The formation of α-eleostearic acid methyl esters was run under basic conditions and has a very similar reaction mechanism to that of the fatty acid saponification reaction. Catalytic amounts of NaOH are required for the methoxide to be formed via an acid-base reaction. The hydroxide in NaOH deprotonates methanol resulting in water (H_2O) and an alkoxide, methoxide. Methoxide attacks the carbonyl carbon, breaking the π bond, and pushing the electrons onto the electronegative oxygen. The tetrahedral intermediate is formed and quickly dissociates, reforming the π bond, and consequently breaking the acyl group carbon and the glycerol backbone oxygen bond. Once the reaction is complete, the resulting products are glycerol and 3 methyl ester chains.

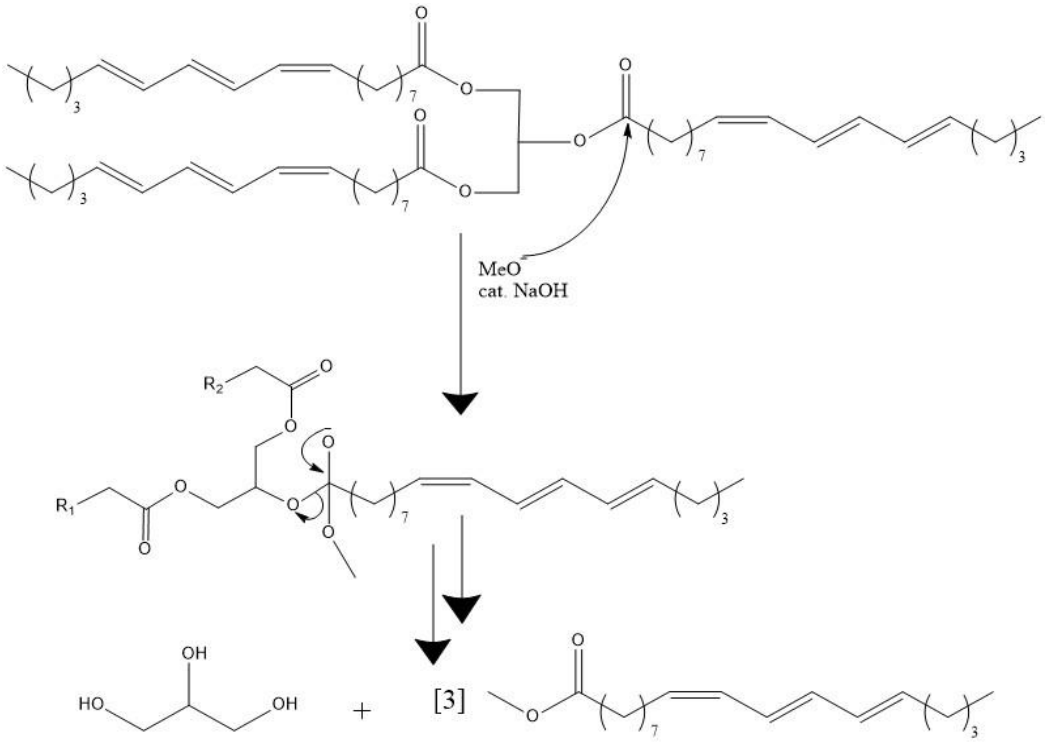

Figure 8. Transesterification of tung oil under basic conditions.

2.4 FATTY ACID AND METHYL ESTER CHARACTERIZATION

Fatty acid extractions, synthesized methyl esters, and tung oil were analyzed by gas-chromatography mass spectrometry (GC-MS), proton nuclear magnetic resonance (^{1}H NMR), raman spectrometry (raman), and fourier transform infrared spectroscopy (FT-IR). Fatty acid samples for GC-MS were prepared by dissolving 0.5 g of fatty acid into 10 mL of acetone, then 3 µL of the fatty acid solution was injected into the GC-MS. For the methyl ester and tung oil analyses, 0.5 mL of the compound of interest was mixed into 10 mL of acetone. Then 3 µL of the diluted solution was injected into the GC-MS. For the methyl ester and tung oil ^{1}H NMR analyses, one drop of the compound of interest, equating to 100 -300 µL, was diluted with around 2 mL or half of the volume of the NMR tube with deuterated chloroform (chloroform-D). The fatty acid ^{1}H NMR sample was prepared by dissolving 1 mg of fatty acid into around 2 mL or half of the volume of the NMR tube with chloroform-D. The sample preparation for raman and FT-IR are more direct. For raman, the compound of interest was secured on a glass slide and the microscope was brought into focused before analysis could begin. In the FT-IR analyses, an ATR accessory was used.

2.4.1 INFRARED SPECTROSCOPY ANALYSIS

In the methyl ester, fatty acid, and tung oil spectra, the weak peaks above 3000 cm^{-1} correspond to the alkene stretch vibrations. The peaks between 3000 cm^{-1} and 2800 cm^{-1} represent the alkane stretch vibrations. There are two other significant peaks to notate, indicating successful extraction of fatty acids and synthesis of methyl esters. The first is a strong peak at around 1750 cm^{-1} representing the carbonyl, carbon-oxygen stretch in the ester (tung oil and methyl ester) or carboxylate (fatty acid) end functional group. The second noteworthy wavelength is a strong peak at around 1000 cm^{-1} which correlates to the carbon-oxygen single bond stretch. The medium peak

around 1480 cm^{-1} represents the sp^3 carbon-hydrogen bending vibration in all three spectra. In the fatty acid and tung oil spectra, the peak below 1000 cm^{-1}, at around 990-980 cm^{-1}, represents the carbon-hydrogen wagging vibrations of the conjugated C-C double bonds (cis, trans, trans). These conjugated C-C double bonds IR peaks in tung oil are commonly seen in other literature[58]. In the methyl ester spectrum, the conjugated C-C double bond peak at 990-980 cm^{-1} is not as prominent as in the other spectra, potentially indicating a loss of C-C double bond conjugation. In conclusion, the three spectra share similarities, and are free of any major impurities. Ultimately, indicating successful extraction and isolation. Further diagnostics with ^1H NMR and bond integration discussed in the following section provides further insight into reaction completion and product purity.

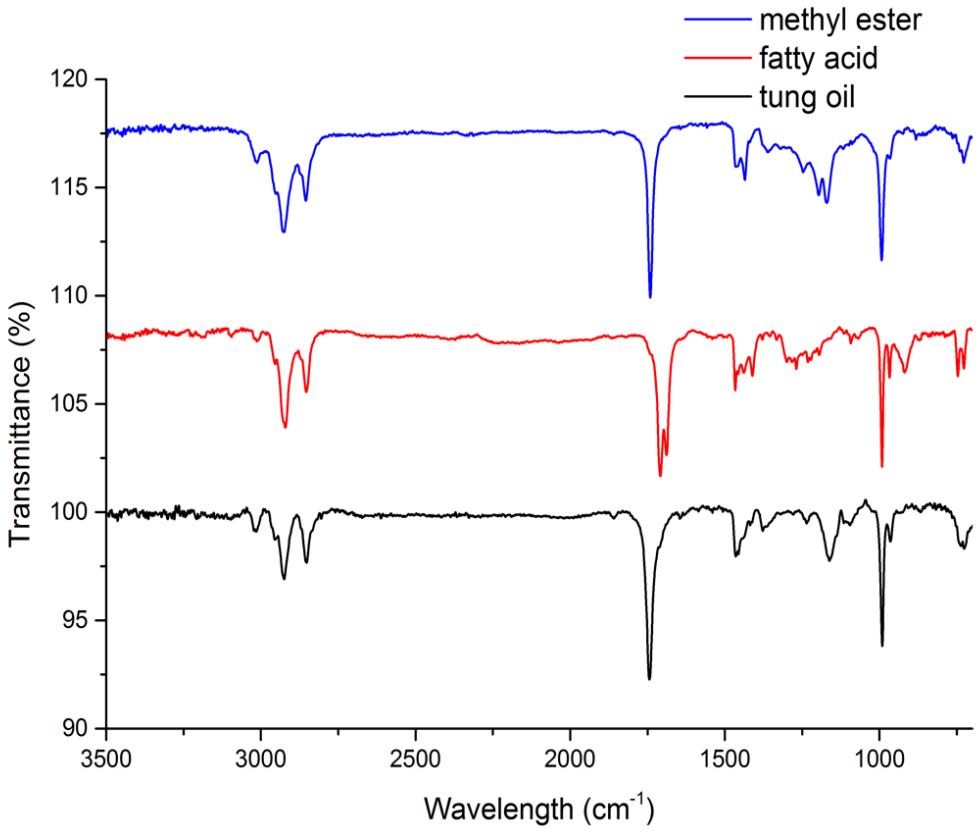

Figure 9. FT-IR of methyl esters, fatty acid and tung oil.

2.4.2 PROTON NUCLEAR MAGNETIC RESONANCE ANALYSIS

In the ^{1}H NMR analyses, tung oil is used as the main reference material to ensure the methyl ester and fatty acid reactions went to completion because it is the only unadulterated starting material. At around 0.5-1 ppm there is a triplet corresponding to the end methyl group on ω-carbon, carbon 18 of the hydrocarbon chain. Around 1.3 ppm, the peak labeled 2 represents the 6 sp^3 hydrocarbons (12 hydrogen) that are connected to other sp^3 carbons. Further downfield, is the peak labeled 3 at around 1.6 ppm which represents the hydrogens attached to the adjacent carbon from the ester group α-carbon. The ester group α-carbon hydrogens represent peak labeled 5 at around 2.3 ppm. Two of the most important peaks in this section to recognize are the glycerol backbone hydrogens which are represented as two separate peaks. The more upfield peak at 4.2 ppm is labeled as peak 4, and corresponds to the two hydrogens attached to the end carbons of the glycerol backbone. The one hydrogen off the middle carbon in the glycerol backbone is found more downfield, at around 5.2 ppm and is labeled 7. Recognizing the absence of these peaks becomes imperative when analyzing the extracted fatty acid and synthesized methyl esters. The methyl ester spectrum has an intense peak at 3.5 ppm representing the newly formed methyl group on the fatty acyl chain. Additionally, with the absence of a peak at 4.2 ppm, illustrating the successful separation from the glycerol backbone, the methyl ester of α-eleostearic acid synthesis can be determined successful. In the fatty acid spectrum, the absence of a peak at 3.5 ppm and 4.2 ppm, suggest a successful drying from the rotary evaporation, and successful extraction from tung oil, respectively.

The next noteworthy peaks are the hydrogens that are connected to the olefin carbons. These peaks are labeled as 8 and range from around 5.3 ppm to 6.4 ppm. It is important that these peaks stay intact since the starting materials undergo a free radical polymerization mechanism,

which requires the presence of double bonds and is described in further detail in the following chapter. The corresponding peaks from the olefin hydrogens, labeled 8 on the tung oil spectrum, were integrated in each of the spectrum with respect to the hydrogens connected to the end methyl group, ω-carbon, of the hydrocarbon chain. In the tung oil spectrum, the integration represents 6 hydrogens from the carbons 8-13. Therefore, indicating that all three C-C double bonds were present. Any large deviations found in the methyl ester and fatty acid integrations would most likely represent the olefins reacting in the extraction and synthesis reactions. In the methyl ester integration, the ratio was found to correspond to 6 hydrogens, also indicating an intact double bond system. For the fatty acid integration, the ratio equated to 5 hydrogens, indicating that this system contained the most double bonds. Despite the differences in integration between the three samples, the overall ^{1}H NMR data showed promising results and complemented the FT-IR analyses. The largest difference in integration was around to equate to 1 to 2 hydrogens, one π bond between the fatty acid and tung oil. As mentioned in chapter 1, tung oil is composed of mostly α-eleostearic acid, a conjugated triene. There is a small percentage of fatty acid chains in tung oil that are saturated, or monounsaturated, and the concentration of these chains are variable between tung oil extracts. This aspect can account for the deviations found the in ^{1}H NMR integrations.

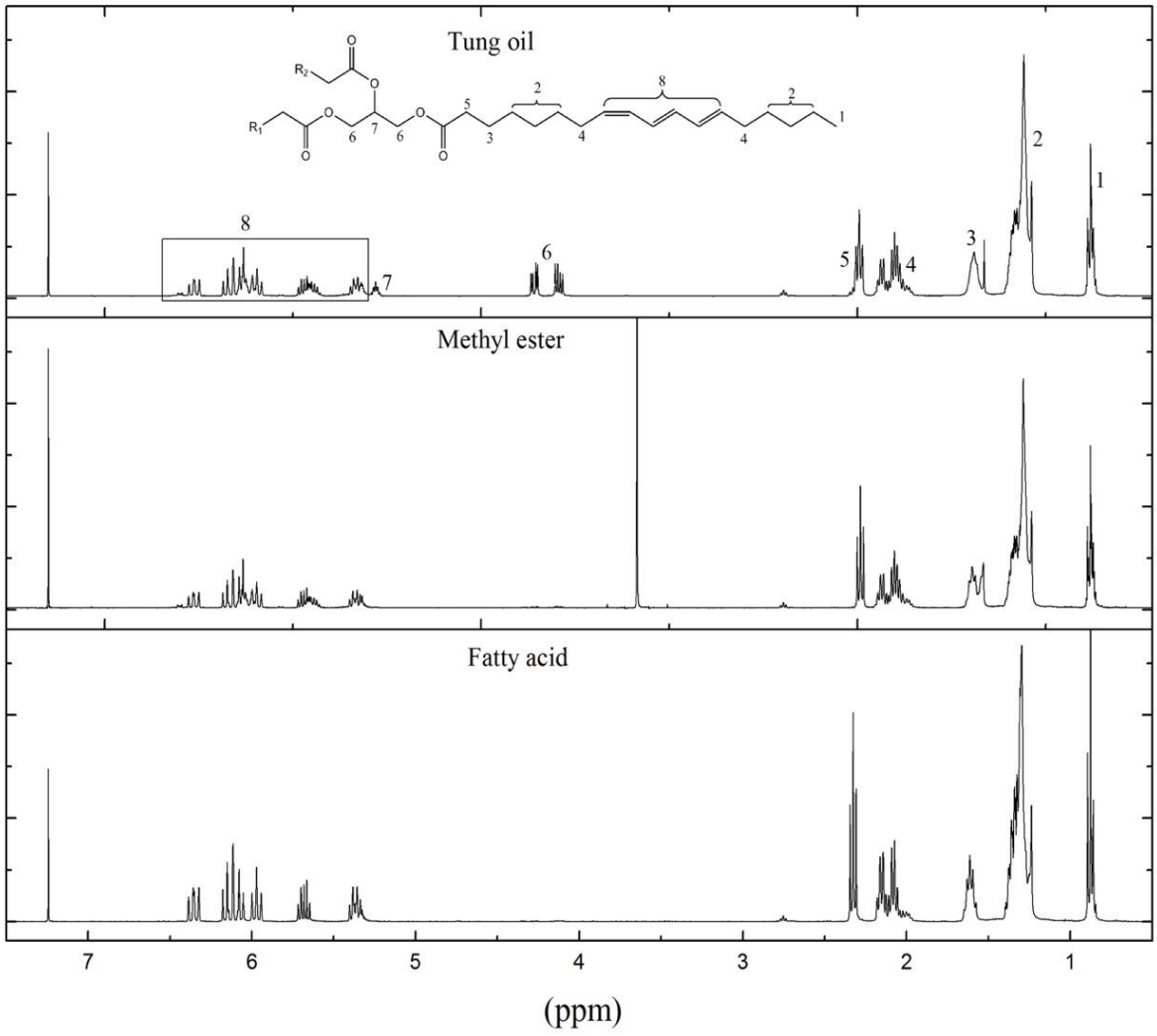

Figure 10. ^{1}H NMR of tung oil, methyl ester (methyl ester of α-eleostearic acid), and fatty acid (α-eleostearic acid) in chloroform-D.

2.4.3 RAMAN SPECTROSCOPY ANALYSIS

In each of the Raman spectrum of the three samples, there are intense peaks at around 1600 cm^{-1} which is standard representation of the carbon-carbon double bonds. The other peaks in the spectra are not as prominent as the alkene peak. Which could be due to the fluorescence of the spectra masking the intensity of the peaks. Overall, the data from the raman spectra, along with the FT-IR spectra, and ^{1}H NMR integrations, displayed evidence that the C-C double bonds

remained intact throughout the extraction and isolation reactions, allowing the research to continue. The next step was to analyze the purity of the sample by GC-MS which is discussed in the following section.

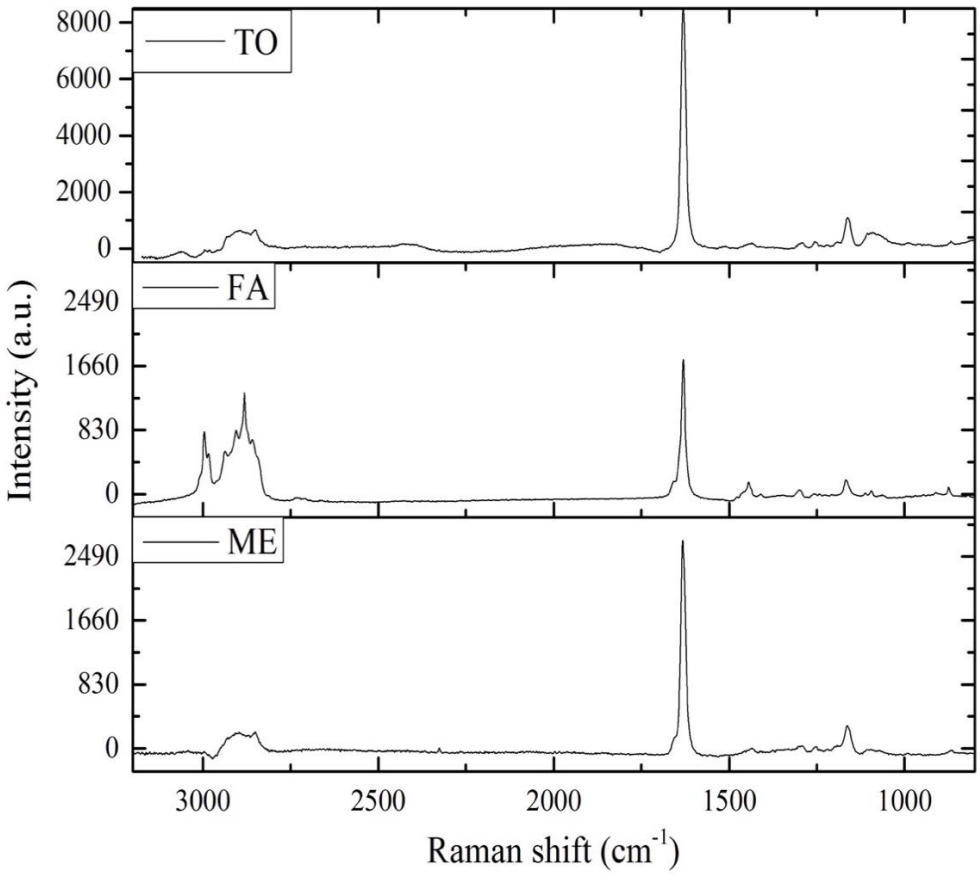

Figure 11. Raman spectra of tung oil (TO), fatty acid (FA), and methyl ester (ME).

2.4.4 GAS CHROMATOGRAPHY ANALYSIS

Gas-Chromatography (GC) is commonly used in sample identification and quantification analyses by the separation of the different volatile components through vaporization. In this manuscript helium is used as the mobile phase inert gas carrier. The sample is carried by the gaseous stream of helium to the column. All components are measured by a detector as they exit the column. Based on the component interactions with the column, some components elude faster

than others. If there are favorable interactions with the column, the sample eludes at a slower time than those with unfavorable interactions.

Based on the retention times and relative concentrations (Table 1) of the peaks from the methyl ester, fatty acid, and tung oil samples, the compounds were mostly composed of one or two peaks. In fatty acid and tung oil samples, there was a major peak present, representing 99% of the relative intensity when integrated. The similarity of peaks between the three samples illustrates that the samples are majority made up of the same components. Which is not surprising, given that there are only subtle differences between the samples, hence why they can be used in comparison to one another. All three compounds are composed of mostly α-eleostearic acid, a long, hydrophobic, 18 hydrocarbon chain. The manipulation of the starting material from an ester to carboxylic acid or carboxylate, at the acyl head is not going to affect the boiling point significantly, which is supported by the relative concentration integrations in the GC analyses of the starting materials. Tung oil displays a small peak at 7-8 mins which is representative of a small fraction of the glycerol backbone eluding from the column. To verify the glycerol peak claim in tung oil, pure glycerol was run through the column. In the glycerol analysis, a broad peak was found at 7-10 mins (Figure 13). In the methyl ester or fatty acid analyses this broad glycerol peak is not found. Thus, complementing the data from FT-IR, ^{1}H NMR, and Raman that the extraction, synthesis and then isolation of methyl esters and fatty acid was successful.

	Peak#	**Retention Time (mins)**	**Relative Intensity**
FA	1	15.794	0.61
	2	16.902	99.39
ME	1	16.277	76.58
	2	16.557	23.42
TO	1	7.855	0.57
	2	16.735	99.43

Table 1. Relative concentration of the integrated peaks in fatty acid (FA), methyl ester (ME), and tung oil (TO) GC samples.

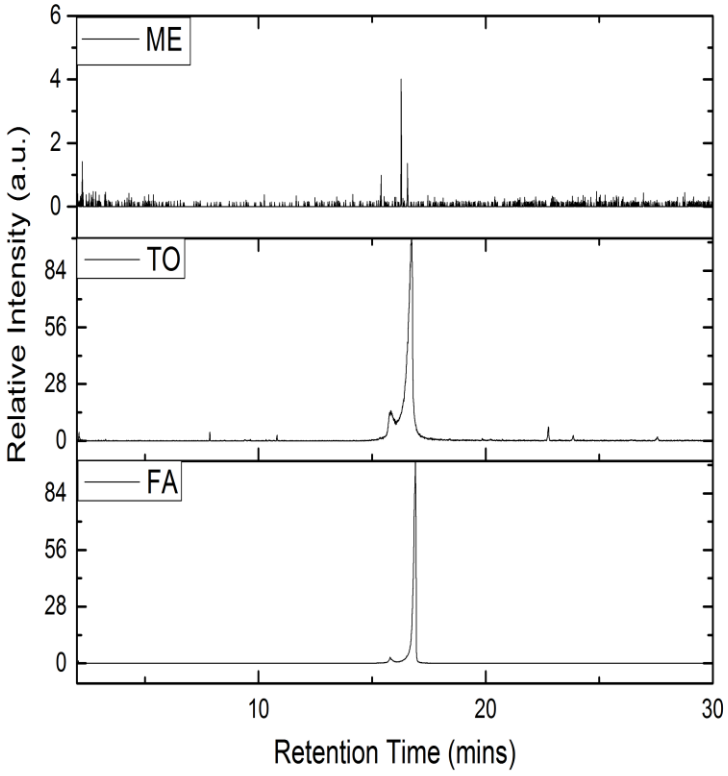

Figure 12. GC of methyl ester (ME), tung oil (TO), and fatty acid (FA)

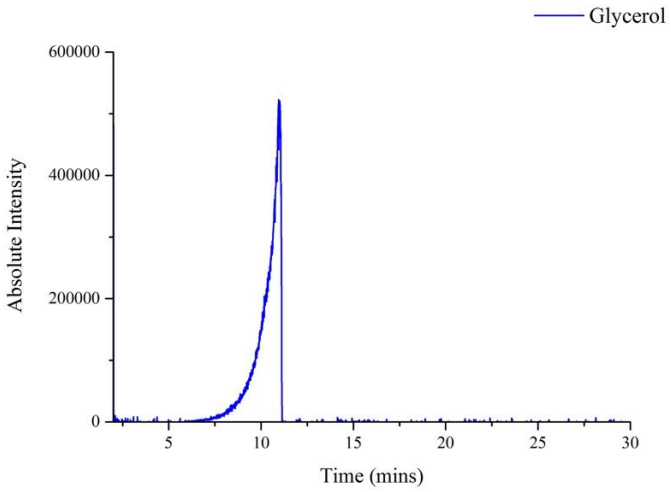

Figure 13. GC of glycerol.

CHAPTER 3: RESIN POLYMERIZATION VIA FREE RADICAL MECHANISM

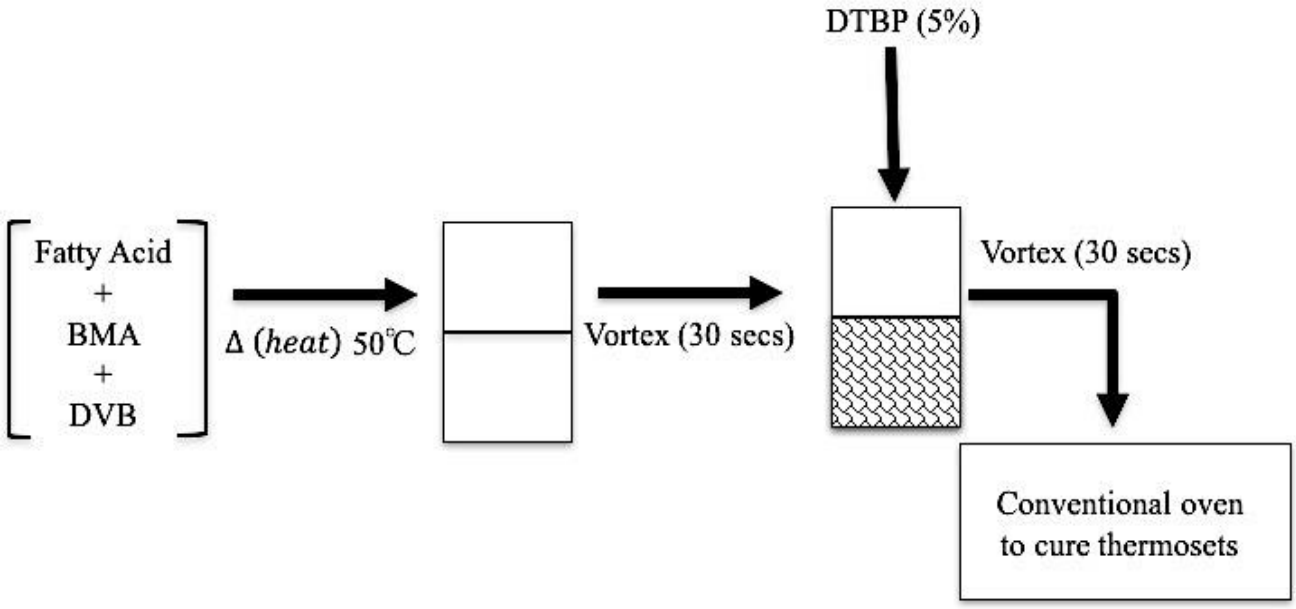

Figure 14. Schematic of the resin preparation cured in a convection oven under air. Tung oil and methyl ester resins were cured in an identical fashion except for the initial heating at 50°C.

3.1 MATERIALS

n-butyl methacrylate (BMA), tung oil (TO), and di-*tert*-butyl peroxide (DTBP) were purchased from Sigma-Aldrich (St. Louis, MO). 80% *p*-Divinylbenzene (DVB) (composed of meta, para and ortho isomers) was purchased from TCI America (Portland, OR). Dielectric analysis (DEA) measurements were completed on an Epsilon DEA 230/1 cure monitor (Netzsch Instruments. North America LLC, Burlington, MA). Raman studies were analyzed on a DXR Raman Microscope (Thermo Scientific, Waltham, MA). Differential scanning calorimetry (DSC) studies were conducted on a Q250 DSC instrument from TA Instruments, New Castle, DE, 5-10 mg of sample were heated from -30°C to 200°C at a rate of 10°C/min. The morphology analyses were completed on a JSM-760F Field Emission Scanning Electron Microscope (JEOL, Peabody, MA), using an accelerating voltage of 1.0 kV, secondary electron imaging (SEI) mode, and an emission

current of approximately 81 mA. The mechanical properties were analyzed on a Q800 DMA (TA Instruments, New Castle, DE) using a three-point bending fixture with a 15 mm gap. Rectangular samples (1.5 x 10.0 x 17.0 mm – thickness x width x length) were cut and subjected to an iso-strain experiment with an amplitude of 14 μm. The temperature was increased from -60°C to 150°C at a heating rate of 3°C /min. The thermal properties were studied on a Q50 thermal gravimetric analyzer (TA Instruments, New Castle, DE) using samples of approximately 10 mg. The experiments were performed under air, from room temperature to 500°C at the heating rates indicated in the text. The resin wettability properties were obtained by a contact-angle goniometer (ramé-hart, Succasunna, NJ) utilizing an automatic drop dispenser.

3.2 RESIN PREPARATION

Fatty acid resins were prepared by heating 5.0 g of the fatty acid extracted from tung oil, 3.0 g of BMA (Figure 15A), and 2.0 g of DVB (Figure 15B) in a 20.0 mL scintillation vial at 50°C until the fatty acid was completely molten. The solution was then vortexed for 30 seconds before 0.5 g of the free radical initiator, di-*tert* butyl peroxide (DTBP), was introduced. The monomer mixture was vortexed again for an additional 30 seconds to create a fully homogeneous mixture. The polymer solution was then placed in the convection oven for the designated temperatures and times, as discussed in the following section. Methyl ester- and tung oil-based resins were prepared identically, with the exception of the initial heating step at 50°C. Indeed, tung oil and the methyl esters are liquid at room temperature, and the initial heating step to create a homogenous mixture applied to fatty acids was not necessary with the other two starting materials. Figure 16 displays a general schematic of the free radical polymerization initiated by heat and the free radical initiator, DTBP. For simplicity, BMA and DVB were not included in the reaction scheme, but are incorporated into the polymer network in the same mechanism as shown in the Figure 16. In the

presence of a radical, the carbon-carbon double bonds will break and share one of their electrons with the radical, forming a new covalent bond. Consequently, a radical is formed on the adjacent carbon from other electron generated from the π system and the polymerization continues until termination.

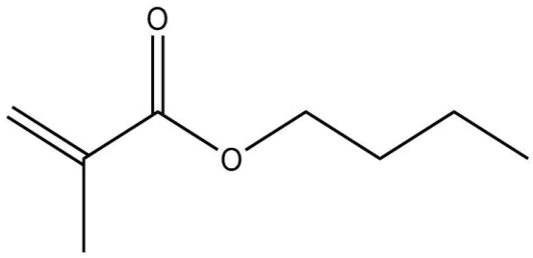

(A)

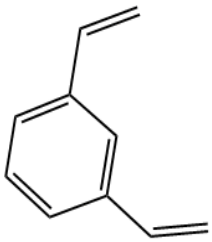

(B)

Figure 15. Chemical structure of **(A)** *n*-butyl methacrylate (BMA), and **(B)** divinylbenzene (DVB) in the meta position.

Both DVB and BMA make ideal candidates for free radical polymerization due to their reactivity. The vinyl olefins in these monomers give rise to ideal reactive sites. In the absence of reactive co-monomers, the internal fatty acid olefins exhibit an exceedingly low polymerization rate, leading to low conversion and poor properties.[59] DVB's π system resonance with the aromatic ring stabilizes radical intermediates/transition states increasing the reaction rate. Likewise, BMA contains an ester functional group conjugated to the vinyl olefin. The electron withdrawing properties of the ester group enhance the reactivity of the olefin. The ultimate resin composition was extensively studied in the recent studies in Johns et al. (2015), providing a fundamental basis into the appropriate monomer compositions leading to this research's final determination of the best ratios. The next decision was to the determine the optimal cure schedule, as will be discussed in sections 3.3.1 and 3.3.3.

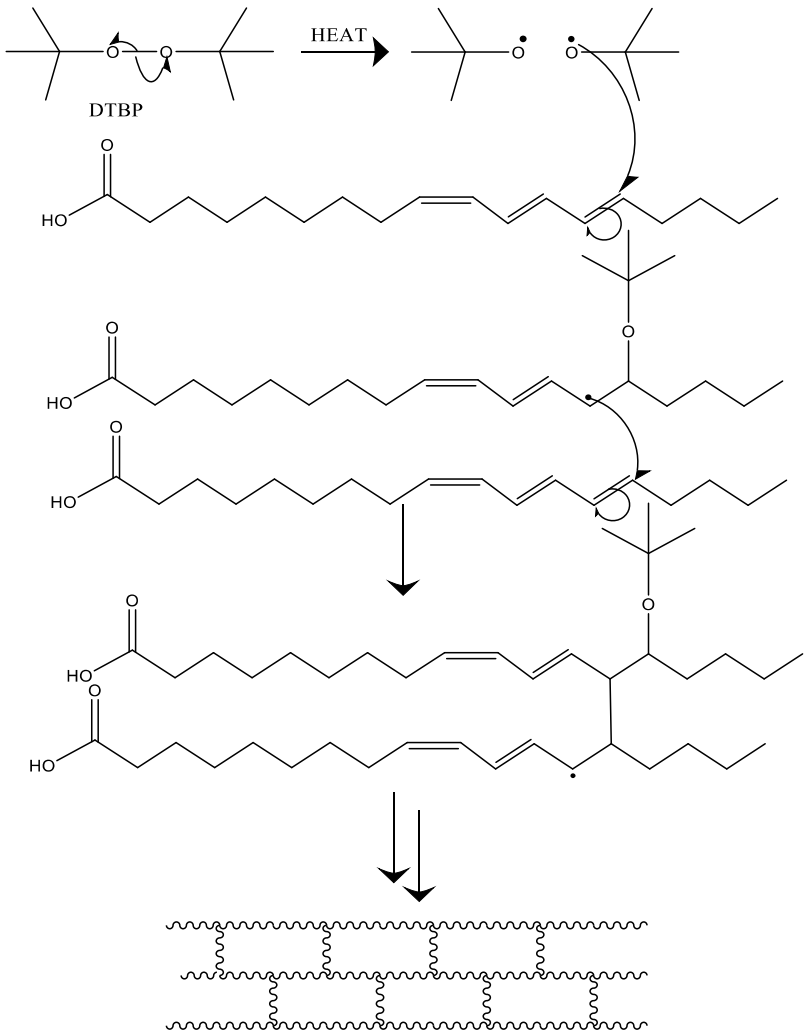

Figure 16. General schematic of free radical polymerization with di-*tert* butyl peroxide (DTBP) as the free radical initiator. For simplicity, cross-linking agents, BMA and DVB are not included in the diagram.

3.3 RESIN CURE CHARACTERIZATION

In previous literature, various amounts of bio-based monomers have been used in combination with petroleum based monomers like DVB or BMA, to create co-polymers with viable and competitive properties. The vegetable oil weight percentage compositions in these co-polymers range from 40% to 70 %. Normally, vegetable oils are not as reactive as their petroleum counterparts. Hence, the creation of hybrid polymers composed of biorenewable starting materials

and petroleum-based products. When establishing the resin composition, it is important to account for the differences in reactivity which will affect the resulting polymer's morphology, and subsequently, the mechanical properties. In this project, it was found that the best combination of monomers was 50% fatty acid, 20% DVB, and 30% BMA (composition [A]). Also, Johns et al. (2013), discovered similar results regarding the DVB and BMA monomer ratios. Other slight variations in composition were deemed successful (Supplemental data, Table 2), and are further discussed in section 3.3.3. The methyl ester and tung oil-based polymers were prepared according to composition [A] to limit extraneous variables for comparison studies. Also, the analytical studies of the cure schedule were completed with polymers of composition [A].

3.3.1 OPTIMIZATION OF CURE SCHEDULE VIA DIELECTRIC ANALYSIS

Dielectric analysis (DEA) cure monitoring takes advantage of a material's electrical permittivity and translates the information into data that can be used to infer the progress of the polymerization reaction. The technique relies on an electrical circuit containing a set of small parallel lines. During analysis, the sensor with the embedded circuit is completely submerged within the sample of interest. An electric current is applied to the circuit, causing any ions within the sample to migrate locally between the circuit lines. By measuring how easily a charge moves within the sample, the resistivity and permittivity of the material can be obtained and correlated to the overall extent of cure of the material, based on the idea that the closer to cure completion, the harder it is for a charge to dislocate through the polymer chains. Regarding thermosetting polymers, the reaction starts off as a liquid with high charge mobility, resulting in low resistivity. As the reaction progresses, the polymer becomes more rigid and crosslinked, consequently causing a decrease in the mobility of ions, which is referred to as "ion viscosity" in the text.[60]

Initially, within the first hour of the cure process of resin [A] (Figure 17), the ion viscosity decreases as the temperature increases. The temperature continues to increase until the desired cure temperature has been reached (120°C, 130°C, or 140°C). After the desired cure temperature is attained, an isothermal is maintained for 20 hours. The initial ion viscosity decrease observed is relative to the initial increase in temperature before polymerization starts, when higher temperatures lead to greater chain movement. Once the polymerization reaction begins (at approximately 1 hour), an increase in ion viscosity is observed due to the growing polymer crosslinked network. Once the ion viscosity plateaus, it is accepted that no further changes occur in the material's electrical and physical properties, indicating cure completion. In this research, the original ion viscosity graph (Figure 17A) continuously increase throughout the duration of the experiment (20 hours). Curing the sample at 140°C lead to significant amounts of shrink cracks, indicating an inappropriate cure temperature. Additionally, the DEA curve obtained at 140°C displayed a secondary decrease in ion viscosity at approximately 12 hours, which is most likely due to exposure of the DEA sensor to air after formation of shrink cracks in the polymer, affecting the permittivity measured.

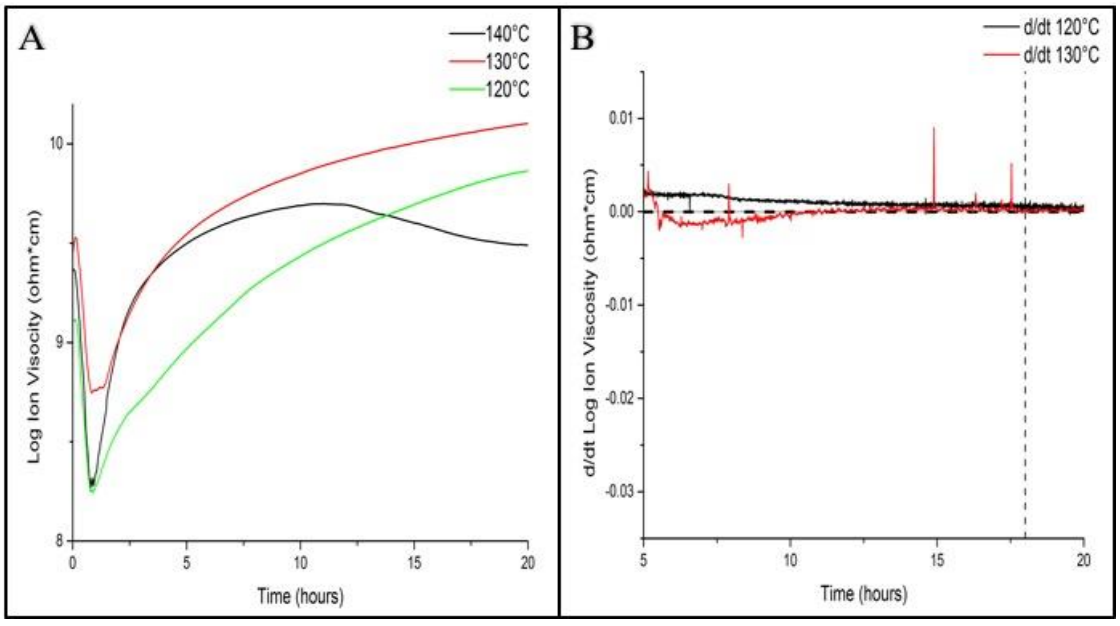

Figure 17. (A) is the DEA analysis run at 140°C, 130°C, and 120°C for 20 hours with a 30 minutes pre-heating time of resin composition [A]. (B) is the derivative of 130°C, and 120°C curves with respect to time of resin composition [A].

The derivative was taken of ion viscosity with respect to time of 120°C and 130°C analyses to determine when the derivative of the slope approaches zero (Figure 17B); indicating the rate of change in the electrical and physical properties is zero. At this point, the polymer is determined to be fully cured. The 130°C cure reaches of slope of zero at around 18 hours. While the 120°C cure reaches zero, later, at around 19 hours. The y-axis of the DEA graph is the log of ion viscosity, therefore, even the slightest changes in electrical properties are detected. It is possible that the changes in electrical properties are due to the polarity of the polymer and the polarization response of those polar functional groups when an electric field is applied. Other studies have discovered that polar polymers display conductivity changes in the pre-melt solid state phase that non-polar, long alkane chain polymers did not display.[61] It was concluded that the increase in conductivity was due to the pre-stressing or polarization of the polar groups in the polymers. Although in this research, the rigidity of the crosslink network should restrict the mobility of the ions, it is certainly possible that a similar phenomenon is occurring as stated in the previously mentioned study.

DEA is more sensitive than DSC and Raman, therefore it is possible that the increase in ion viscosity is directly related to the slowly growing polymer chain, and that there are some remaining unreacted materials left within the polymer. Before any definite conclusions can be made regarding the continuously increasing ion viscosity slope, further investigations must be done. Concerning the optimization of the cure schedule, taking the derivative of the slope is efficient enough for this research when determining the end of cure. Further complementary analyses with DSC and Raman are discussed in the following section 3.3.2 to confirm cure

completion. Since tung oil and methyl ester resins are used for comparison purposes, it was more appropriate to utilize the same cure schedule as the fatty acid based resin to eliminate any extraneous factors that could affect the thermo-mechanical properties. Optimizing the cure schedule of the tung oil and methyl ester resins was not part of the central focus of this research, but could be interesting to explore in future research.

3.3.2 CURE VERIFICATION VIA DIFFERENTIAL SCANNING CALORIMETRY AND RAMAN SPECTROMETRY ANALYSIS

Differential scanning calorimetry (DSC) is a commonly used thermal analysis technique that measures the difference in heat flow between the polymer sample and empty reference pan with respect to temperature. The sample pan and reference pan are heated, cooled or held isothermally, and the respective heat flow differences are recorded. DSC analyses allow users to obtain a thorough understanding of the cure kinetics and process. Dependent on the chemical processes taking place during the analysis, the sample can either absorb or release heat/energy to maintain its heating rate equilibrium with the reference pan. This energy release or absorption trend plots nicely on the DSC graph as an exothermic or endothermic peak. An absence of an exothermic peak can be an indication of a fully cured sample. If the polymer was not fully cured, the heat from the DSC analysis would regenerate the polymerization reaction, resulting in exothermic peaks on the DSC curves. Exothermic peaks can also be indicators of the polymer crystallizing. While endothermic curve shifts are more likely to be indicators of a glass transition temperature (T_g), or the polymer melting. From the measurements of the heat flow as a function of time, the enthalpy can be obtained by integrating the area of exothermic or endothermic peaks.

To confirm the DEA data, and polymerization completion, as well as to explore the cure thermal properties further; the tung oil (TO), fatty acid (FA), and methyl ester (ME) resins were

evaluated by DSC (Figure 18A). In the DSC analyses, the tung oil and fatty acid resins are fully cured based on the absence of exothermic peaks. On the other hand, the methyl ester resin DSC curve displays a large exothermic peak onset at around 117°C, indicative of an uncured sample. Thus, indicating the methyl ester resin representing the least reactive of the three polymers. Around 115°C, both the tung oil and fatty acid resins contain an endothermic shift on the DSC curve representing sample degradation or the glass transition temperature (T_g). Further analysis with DMA and TGA can further explain the phase changes and are discussed in their respective sections, 3.4 and 3.5.

Raman spectroscopy is a complementary technique to FT-IR that measures the rotational and vibrational transitions in molecules to detect chemical bonds. When used in-situ, it can be used for monitoring the progression of a reaction.[62] Raman spectrometry is particularly known for its intense signals for carbon-carbon double bonds which appear at around 1600 cm^{-1}. The polymerization reaction mechanism used in this research is a free radical mechanism, which utilizes the double bonds present in the polymer to build its crosslink network. Therefore, any carbon-carbon double bonds signal produced on the Raman spectrum, would be an indication that the reaction did not go to completion. Although, it is impossible for all the double bonds to be 100% reacted, which is a limitation of utilizing the free radical polymerization mechanism. It is important for the cure to be brought to completion as much as possible, to avoid any unwanted side reactions occurring or early onset of polymer degradation.

The Raman spectra of fatty acid resin composition [A] (the determined ideal polymer composition) and a partial polymerized resin, composition [L] (7 g FA, 1 g DVB, 2 g BMA), were evaluated for the presence of carbon-carbon double bonds (Figure 18B). At room temperature, the resin [L] was tacky and liquidity, which could be an indication that the polymer

had a very low T_g. Although, the more likely explanation is that the tackiness, and liquid like state is due to the polymerization reaction not going to completion. Thus, making resin [L] an ideal candidate to explore if the Raman laser was at the right conditions to distinguish between the background noise wavelengths and the wavelength peak for the carbon-carbon double bond. In the resin [L] Raman spectrum, labeled un-polymerized resin, there is a distinct peak at around 1600 cm^{-1}, indicating the presence of carbon-carbon double bonds. In the resin [A] spectrum, the peak is absent, indicating that the polymer was fully cured as previously supported by DSC and DEA. Overall, based on the DEA, DSC, and Raman analyses, the optimal cure schedule was successfully determined to be: room temperature to 130°C (pre-heating time) in 30 mins, and then isothermally cured at 130°C for 18 hours. Surface morphology studies are discussed in the following section 3.3.3, to confirm the optimal monomer feeding ratios in order to produce a polymer free of fractures or cracks, that would otherwise diminish the thermo-mechanical properties.

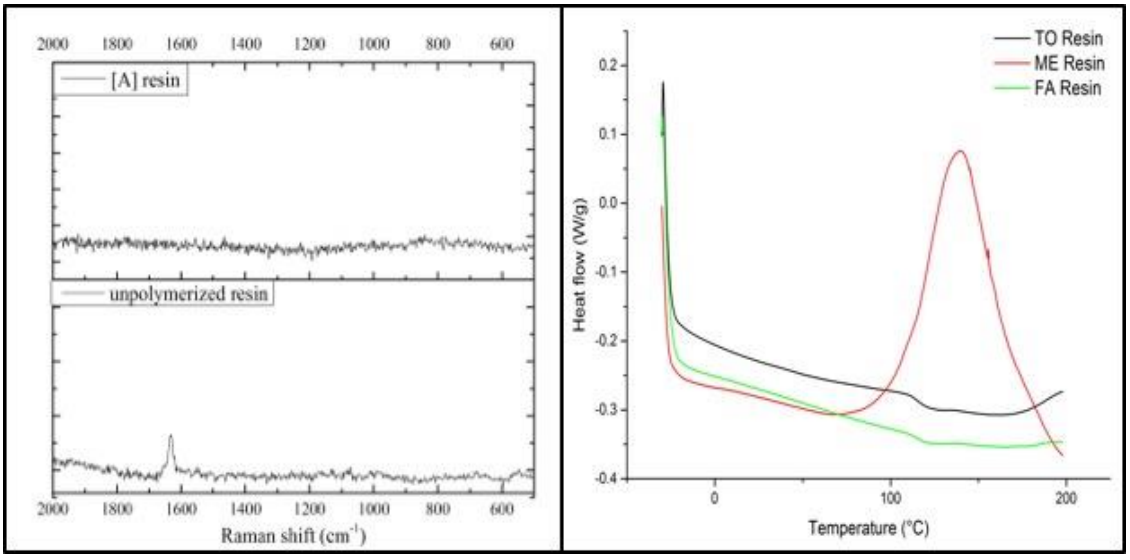

Figure 18. **(A)** Raman spectra of composition [A] and a partially polymerized resin (composition [L]). **(B)** DSC experiments run under nitrogen from -30°C to 200°C at a rate of 10°C/min for composition [A] of fatty acid, tung oil, and methyl ester based resins.

3.3.3 MORPHOLOGY ANALYSIS BY SCANNING ELECTRON MICROSCOPE

Further investigations were conducted of the resin surface morphology to ensure proper monomer feeding ratios. The most promising samples were analyzed under a scanning electron microscope (SEM). Initially, visual qualitative studies were conducted to weed out the samples with macro-cracks, bubbles or fractures. Over forty samples were cured, and seven combinations of monomers were determined to have acceptable morphology properties (Supplemental data, Table 2). Out of the seven compositions, three combinations of monomers were selected that had the best contiguity, and greatest difference in monomer composition (Table 3). Resin [NN], resin [A], and resin [Z] were analyzed under SEM to determine if there were any micro-cracks that could potentially affect the mechanical properties. Methyl ester and tung oil resins were cured with the resin composition of [A], since it displayed the best morphology contiguity of all the samples. Based on the SEM images (Figure 19), all five samples are free of cracks, bubbles or fractures, indicating appropriate monomer ratios. Once the monomers ratios were determined, resin [NN], [A], and [Z], methyl ester and tung oil resins are ready for mechanical property evaluations by dynamic mechanical analysis (DMA).

	FA (g)	DVB (g)	BMA (g)
NN	4.5	1	4.5
A	5	2	3
Z	6	3.5	0.5
ME*	5	2	3
TO**	5	2	3

Table 3. Monomer combinations in fatty acid, methyl ester and tung oil resins cured at 130°C for 18 hours. *Methyl ester based resin. **Tung oil based resin.

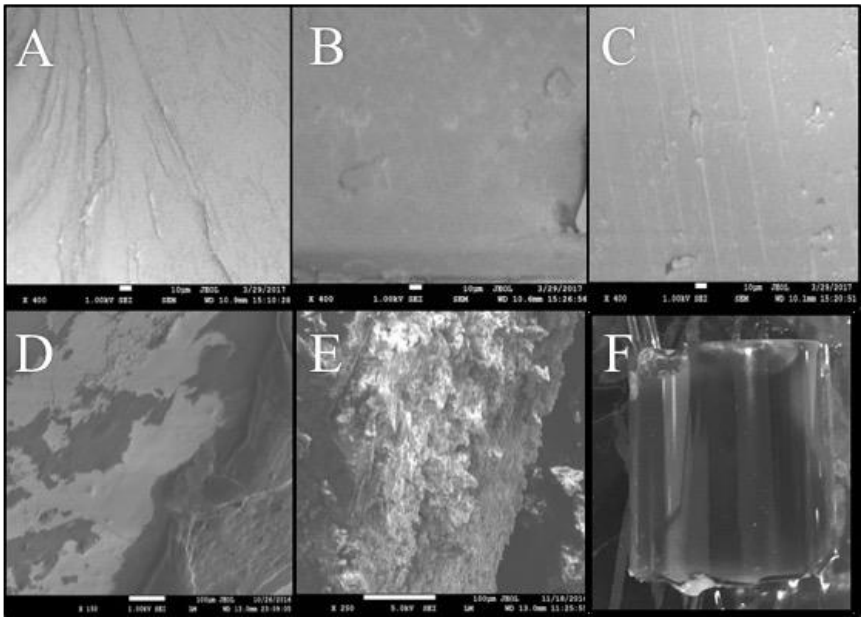

Figure 19. (A) Fatty acid [A] resin. (B) Methyl ester [A] resin. (C) Tung oil [A] resin. (D) Fatty acid [Z] resin. (E) Fatty acid [NN] resin. (F) Fatty acid [A] resin. All samples were cured at 130°C for 18 hours. Samples A-C images were taken with SEM at 400 magnification (x), Image D at 150x, and Image E at 250x, under 1.0 kV accelerating voltage, and SEI detector mode. Image F was taken with 12-megapixal camera.

3.4 RESIN MECHANICAL PROPERTIES

Vegetable oil based co-polymers are commonly used in research due to their tunable mechanical properties by adjusting the resin composition, as well as their inexpensive design. The most conventional mechanical property evaluation is completed on a dynamic mechanical analysis (DMA) instrument. DMA measures the response of the sample to a sinusoidal or an oscillating stress. This stress can be representative of changes in force, temperature, or frequency and sample's respective deformation response. The amount of sample deformation is related to its stiffness or elastic behavior, and is measured by the storage modulus, E' or G'. Under sinusoidal force conditions, the modulus can be divided into two components, an in-phase

component and an out of phase component. The in-phase component is known as the storage modulus and the out of phase component, the loss modulus. The tan δ is the ratio of the loss modulus to the storage modulus, and is often referred to as damping. It is a measurement of the energy dissipated, and an indication of how well the sample can adsorb energy.

DMA experiments were run in a multi-frequency-strain mode, using the three-point bending clamp from -60°C to 150°C at a heating rate of 3°C/min. The analyzed resins behaved as most thermosetting polymers would, under the given conditions exhibiting the three distinct regions of viscoelasticity: glassy state, glass transition state, and rubbery plateau state. At low temperatures, all the resins are in their stiff, glassy states and show little differences in storage modulus until around 0°C as the resins are approaching their glass transition temperatures. As expected, the storage modulus decreases as the temperature increases. From around room temperature, 25°C, to 75°C, there is a sharp decrease in the storage modulus corresponding to the segmental relaxation, as the resins are transitioning from their brittle, glassy states to their glass transition states, and ultimately above their respective T_gs. From around 75°C to end experimental temperature, 150°C, the resins' storage modulus plateaus. This region is known as the rubbery plateau state and is indicative of cross-linked polymers since thermosetting polymers do not melt due to their highly cross-linked networks.

The resin [NN] displayed the weakest mechanical properties of the polymers tested, as well as the most significant decrease in storage modulus as the polymer transitions above its T_g. Overall, as the DVB weight percentage increased in the resins, the storage modulus increased. DVB is a rigid, cross-linker commonly used in co-polymers to increase the mechanical properties. Based on DVB's structural composition, it is not surprising that the storage modulus was enhanced by increased ratios of DVB. DVB has two reactive, vinyl carbon-carbon double

bonds that react in the polymerization reaction, which are attached to an aromatic ring, significantly restricting the subsequent polymer's ability for molecular rotation. The tung oil resin has comparative mechanical properties to that of the fatty acid resin [Z], despite the 15% decrease in DVB composition. Tung oil is a triglyceride that contains a three carbon, glycerol backbone. The glycerol backbone accounts for the increased mechanical strength, by restricting the polymer's molecular movement and therefore, enhancing its rigidity. Resin [A]'s mechanical properties lie between [NN] and [Z], supporting the DVB trend (Figure 20). Additionally, none of the resins display secondary relaxations in the E' curves, indicating a single T_g range and a homogenous mixture. If secondary relaxations, also known as β relaxations, were present in the curves, it could be an indication of multiple T_gs and ultimately, incompatible reactivity within the monomers. Also, multiple T_gs implies a phase separation within the polymers, such as in the case of block co-polymers which have block regions of monomer A and regions of monomer B.

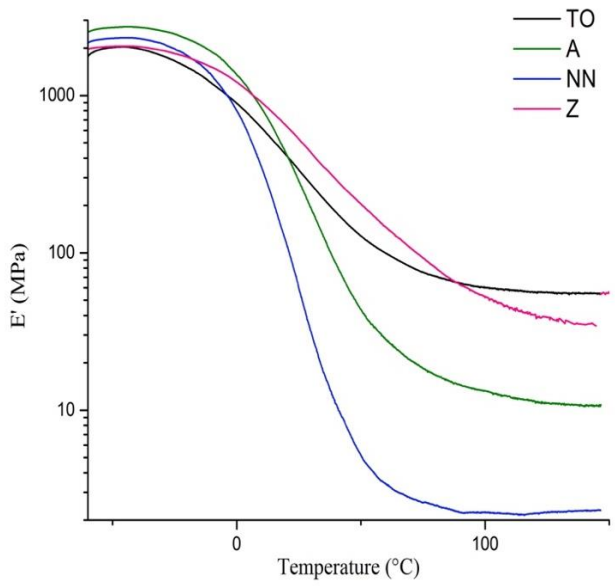

Figure 20. Storage modulus E' curves, evaluated by DMA, of tung oil (TO), fatty acid composition [A] (A), fatty acid composition [NN] (NN), fatty acid composition [Z] (Z) resins.

The width of the tan δ curves also indicate the homogenous or heterogeneous nature of the polymer composition. The wider the tan δ curve, the more heterogeneous the polymer is (Figure 21). The maximum value of the tan δ curve represents the glass transition temperature (T_g). As expected, as the DVB content increases, the T_g increases (Table 4). Consequently, as the DVB content increases, so does the width of the tan δ curve, indicating phase separations. It is not surprising these phase separations occur, DVB is a very hydrophobic and reactive cross-linker. Although, BMA and fatty acid monomers are hydrophobic by nature, they do contain hydrophilic regions within them. For example, the ester group in BMA, and carboxylic acid group in the fatty acid. Despite BMA's vinyl carbon-carbon double bond and carbonyl double bond, the parent chain contains a butyl group (four carbon chain) which acts as a plasticizer to decrease the T_g and rigidity. Similarly, the fatty acid monomer's ability to act as a plasticizer is magnified in comparison to BMA, due its 18-carbon long parent chain. Naturally, since resin [NN] contains the most content of plasticizing agents, and flexibility, it was resin with the highest damping properties (Figure 21). As well as the resin with the lowest T_g. The other fatty acid resins [A] and [Z], followed the inverse trend of the storage modulus. The resin tan δ values are as follows: [NN] > [A] > [Z] ≈ [TO]. Since resins [Z] and [TO] have similar storage modulus, it is not surprising that their damping properties are relatively the same. Both resins are relatively stiff in comparison to resins [NN] and [A].

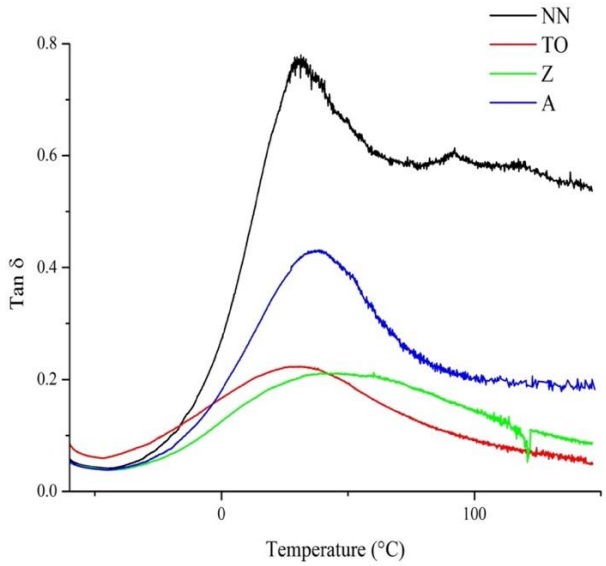

Figure 21. Tan δ curves from DMA of resins.

Exploring the cross-link density can also explain the increased storage modulus and resulting stiffness found in [TO] and [Z] resins. Consequently, allowing for inferences regarding the lowered damping properties as well. Cross-link densities were calculated based on the rubbery elasticity theory.[63, 64] Calculations can be explained by qualitative consideration of the crosslinking density (V_e) of the thermosets, according to rubber elasticity theory, using equation (1). Where E' is the storage modulus at Tg + 50°C, well into the rubbery plateau region. R is the gas constant, 8.3145 $cm^3 * MPa * K^{-1} * mol^{-1}$, and T is the absolute temperature (°K) where the experimental modulus was determined. V_e is expressed as moles of elastically effective network chains per cubic centimeter of resin (Table 4). Similarly, in reference to the fatty acid resins, as the DVB content increases, the cross-link densities significantly increase, explaining the increase in storage modulus and rigidity. [TO] has the highest cross-link density, as expected since it has the highest storage modulus at the temperature of interest. Overall, [TO] had the highest storage modulus above its T_g, and the highest cross-link density. Fatty acids resins'

mechanical properties increased with the increased content of DVB. The methyl ester resin was too soft, and brittle for evaluation. Therefore, it has been excluded from the mechanical property evaluation by DMA.

	FA (g)	**DVB (g)**	**BMA (g)**	**Glass Transition (℃)[a]**	**Storage Modulus E' (25 ℃) [b]**	**Storage Modulus E' (T_g + 50℃) [c]**	**Cross Link Density V_e $\left(\frac{mol}{cm^3} * 10^{-4}\right)$ [d]**
NN	4.5	1.0	4.5	31	58.69 MPa	2.46 MPa	2.78
A	5.0	2.0	3.0	39	284.8 MPa	14.60 MPa	16.16
Z	6.0	3.5	0.5	46	526.5 MPa	56.07 MPa	60.90
ME*	5.0	2.0	3.0	-	-	-	-
TO**	5.0	2.0	3.0	32	338.4 MPa	68.85 MPa	77.72

Table 4. [a] Glass transition temperatures evaluated from the tan δ curves, [b,c] storage modulus from the E' curves, evaluated from the DMA analyses of tung oil (TO), fatty acid composition [A] (A), fatty acid composition [NN] (NN), and fatty acid composition [Z] (Z) resins. [d] Cross link densities calculated the equation, $V_e = E'/3RT$ and E' obtained from DMA.

$$V_e = E'/3RT \quad (1)$$

3.5 RESIN THERMO-STABILITY PROPERTIES

The resins' thermal properties evaluated by TGA were run under air from room temperature to 500°C at various heating rates (2°C/min, 5°C/min, 10°C/min, or 20°C/min). All the co-polymers are thermally stable until around 100°C, with temperature variations (10°C to 40°C) between the start of thermal degradation (Table 5), strongly dependent on the heating rate, and the polymer composition. The polymers exhibit characteristics of a three-stage thermal degradation mechanism above 100°C (Figure 22). The first stage of degradation is from around 100°C to 200°C and represents the evaporation of soluble, unreacted materials, as well as their subsequent decomposition. These materials are the easiest to evaporate/degrade since they are not included in the cross-link network. The second stage is from around 200°C to 450°C, and is

the region with the fastest degradation, expressed by the steepest slope. This degradation stage is representative of the cross-link network degrading. In the last stage from 450°C to 500°C, the degradation slope starts to plateau, as the polymer residue reaches its maximum weight loss, often referred to as char. The last stage degradation corresponds to the steady, oxidative behavior of the char as it evaporates/degrades.

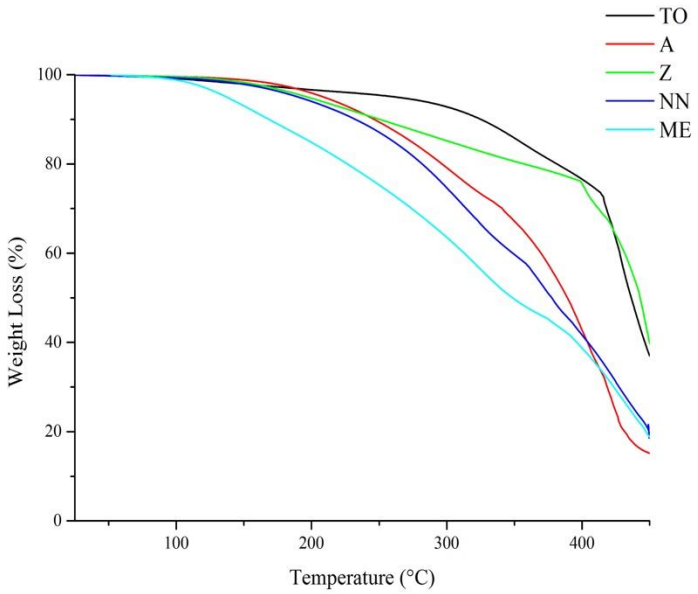

Figure 22. TGA curves of resins from room temperature to 500°C at a heating of 10°C/min.

Based on the results of Table 5, no formal trends can be determined between the fatty acid based polymers ([A], [NN], and [Z]) until after 50% weight loss, well into the cross-link network degradation stage. At T_{50}, as the cross-link densities of the fatty acid based polymer increases ([Z] > [A] > [NN]) (Table 4), the respective degradation temperature increases (Table 5). This trend exhibits characteristics as expected, since the higher the cross-link densities, the more covalent bonds that must be broken for degradation to occur. Between the resin [A] (fatty acid based), resin [TO] (tung oil based), and resin [ME] (methyl ester based), [TO] displayed the most stable thermal properties. The thermal stability trend is as follows: [TO] > [A] > [ME]. A similar trend was found in the mechanical property evaluations from DMA (section 3.4). This

coincidence can be accounted for because of the high cross-link density nature of the [TO] polymer enhancing its thermo-mechanical properties in comparison to [A] and [ME]. [ME] displayed the overall worse thermo-mechanical properties. This decrease in thermo-mechanical properties can be accounted for by the poor reactivity of the methyl ester polymers in comparison to the fatty acid and tung oil polymers.

Despite resin [A]'s low cross-link density, the resin displayed the most stability in regards to the onset of degradation. Most of the co-polymers started degradation around 100°C ± 10 °C, excluding resin [Z]. Interestingly, the resin [A] did not begin degradation until around 144°C. These variations in thermal degradation are accounted for by the uniformity of the resin compositions based on the width of the tan δ curves (Figure 21). [TO] and [Z] are heterogeneous and contain phase separations in comparison to the other polymers ([NN] and [A]). It is possible that the sample analyzed by TGA from [TO], contained an oil-rich phase, therefore, falsely decreasing the onset of degradation, and vice versa for resin [Z]. The sample taken for analysis of resin [Z], could have been a DVB-rich phase, which would degrade at a higher temperature due to its increase in rigidity in comparison to the oil-rich phase. Further analyses in polymer stability are discussed in the following section 3.5.1. These studies measure the degradation activation energy, which considers a variety of heating rates allowing for a better understanding of the degradation kinetics.

	T_{start} (℃)[a]	T_{10} (℃)[b]	T_{20} (℃)[c]	T_{50} (℃)[d]	T_{75} (℃)[e]
NN*	110.57	237.79	287.57	393.01	460.52
A*	144.12	251.35	310.45	430.36	472.14
Z*	128.33	272.45	374.92	458.06	484.47
ME	101.54	202.8	266.05	398.77	462.31
TO	99.80	340.99	396.12	450.82	472.96

Table 5. Thermal degradation temperatures at the [a]start of degradation, 0.5%, [b]10% weight loss, [c]20% weight loss, [d]50% weight loss, and [e]75% weight loss extracted from TGA curves run under air at a heating rate of 10°C/min. *Fatty acid based resins.

3.5.1 RESIN DEGRADATION ACTIVATION ENERGY

To further explore the thermal stabilities of the cured polymers, a simplistic polymer stability experiment evaluated using TGA at four different heating rates (2°C/min, 5°C/min, 10°C/min, and 20°C/min) from room temperature to 500°C under air was conducted. From the different heating rates, temperatures at several isoconversional points (20% wt. loss, 10% wt. loss, and 5% wt. loss) were selected for analysis. The heating rate was set equal to the Arrhenius function, and the resulting equation was manipulated into slope-intercept form. From equation (2) the natural log (ln) of the heating rate (β) was plotted against inverse of the absolute temperature (° K). The slope of the line equates to $-\Delta E_a/R$. Where ΔE_a is the activation energy and R is the universal gas constant (8.314×10^{-3}). To obtain the activation energy, the slope was multiplied by the negative value of the gas constant, resulting in units of kJ/mol.

$$y = mx + b \tag{2}$$

The integrity of this method was verified by basic mathematical kinetic equations derived from the Arrhenius equation (4) and the Law of Mass Action. Kinetic studies can be described by the general rate equation (3). In this equation k is the rate constant, α is the rate of conversion at a constant temperature, and f (α) is the reaction model. In this manuscript, the polymers are assumed to express an nth order conversion function $(1-\alpha)^n$, 1st order linear degradation (n = 1), and α to be proportional to the reactants left. dα/dt is the reaction rate, represented by the derivative of the conversion fraction with respect to time.

$$\frac{d\alpha}{dt} = k * f(\alpha) \quad (3)$$

The Arrhenius equation (4) can be substituted for the rate constant k, yielding the equation (5).

$$k = A \exp\ (-Ea\ /\mathrm{RT}) \quad (4)$$

$$\frac{d\alpha}{dt} = [A \exp\ (-E_a\ /\mathrm{RT})] * f(\alpha) \quad (5)$$

However, during dynamic analyses, the temperatures increases linearly with respect to time, equation (6). Therefore, by introducing the heating rate variable and rearranging equation (6), the resulting relationship with equation (5) equates to equation (7). Equations (5) and (7) are fundamental polymer kinetic equations used in advanced kinetic studies to explore the activation energies, and pre-exponential factor.

$$\beta = \frac{\mathrm{dT}}{\mathrm{dt}} \qquad dt = \frac{dT}{\beta} \quad (6)$$

$$\frac{d\alpha}{dT} = [\frac{A}{\beta} \exp\left(-\frac{E_a}{RT}\right)] * f(\alpha) \quad (7)$$

By rearranging the equation to bring it into slope-intercept form, equation (8) was formed. The natural log of both sides was taken, and the final equation, equation (9) was determined. The y-intercept is represented by $ln\ C$, which is a combination of the reaction model (f (α)), pre-exponential factor (A), and the derivative of the reaction fraction with respect to temperature (T).

$$\frac{d\alpha}{dT}\beta = [A \exp\left(-\frac{E_a}{RT}\right)] * f(\alpha) \quad (8)$$

$$\ln \beta = -\frac{E_a}{R} * \frac{1}{T} + \ln C \quad (9)$$

- $\ln C = \ln\ (f(\alpha) * \frac{d\alpha}{dT} * A)$

To ensure accuracy, isoconversional points were selected with the highest coefficient of determination (R^2) based on the fatty acid resin [A] results (Figure 23). Additionally, qualitative analyses of the linear regression lines of the conversion levels are indicators to whether the

appropriate points were selected. If the regression lines are parallel to one another, then the respective polymers have similar degradation kinetics. The chosen conversion levels are 20% wt. loss, 10% wt. loss and 5% wt. loss. Based on the activation energies listed in Table 6, the [ME] resin had the lowest degradation activation energy, equating to the least stable polymer, and the easiest to degrade. The [TO] resin had the highest degradation activation energy, and was determined to be the most stable of the three polymers. Fascinating enough, Resin [A] had competitive properties with the [TO] polymer. Which potentially could have implications in relation to utilizing the fatty acid resin [A] in replacement of the tung oil resin [TO] when the application required can decrease slightly in the mechanical properties.

Figure 24 displays the graphical trends of the respective polymers as the weight loss, or conversion level increases. Resin [A] and [TO], both show an increase in activation energy as more of the polymer is degraded. Although, the activation energy should relatively remain the same as polymer degrades, the respective polymers have several components that contribute differently to the degradation mechanism. These deviations could be representative of the different monomers degrading or representative of instrumental error. Interestingly, the least stable polymer, resin [ME], degradation activation energies, relatively remained the same throughout evaluation. Which would be an indication that the degradation kinetics are uniform, throughout the evaluation. The [ME] resin contained a certain percentage of unreacted material based on the DSC curves (Figure 18), and a polymerization reaction of the unreacted material could be skewing the initial data. The proposed polymerization could be counteracting the beginning stages of degradation, masking the deviations in data. Overall, the data displayed promising results and agreed with the trends found in the previous section.

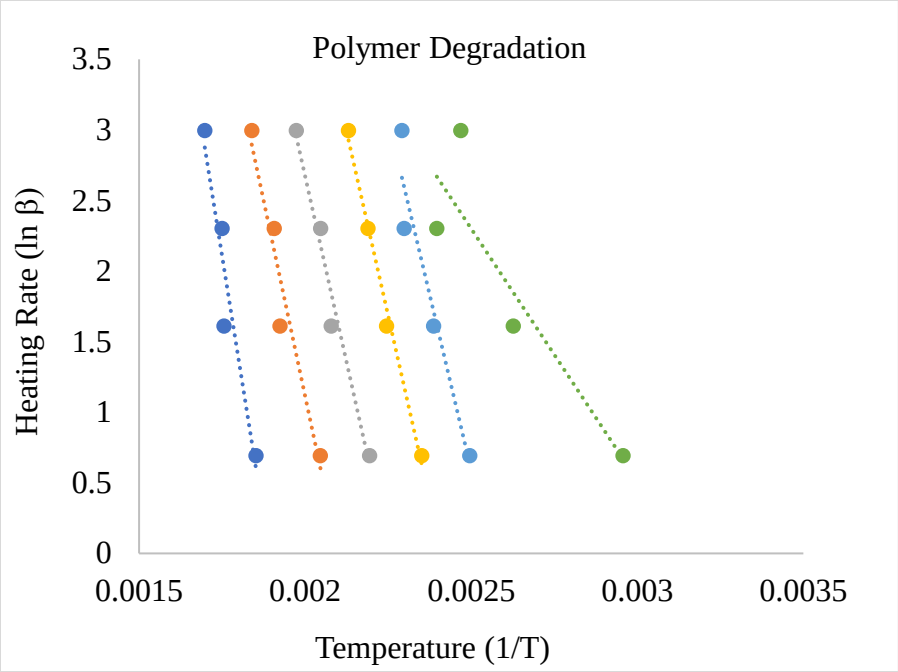

Figure 23. Simple polymer degradation graph (ln heating rate (β) vs 1/T).

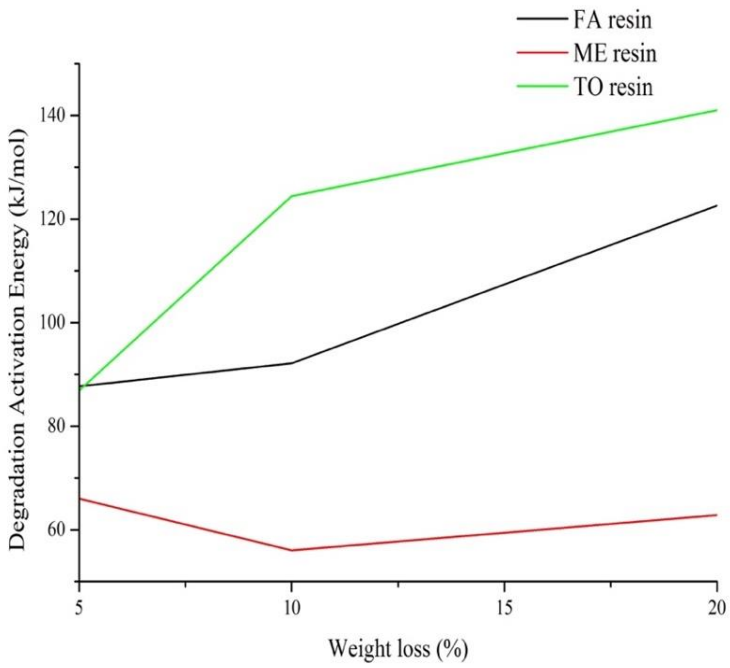

Figure 24. Degradation activation energy graphical trends of resins.

Sample	Weight Loss (%)	Activation Energy (kJ/mol)
FA Resin	20	122.64
	10	92.18
	5	87.73
ME Resin	20	62.86
	10	56.03
	5	66.03
TO Resin	20	141.05
	10	124.44
	5	86.89

Table 6. Degradation activation energies of resins.

3.6 RESIN WETTABILITY PROPERTIES

Wettability measurements are arguably the most widely operated and simple surface analysis technique directly related to the polymer's surface hydrophilicity, coating abilities, and strongly representative of the surface adhesion properties.[65,66] Calculations based on measured contact angle values are commonly utilized for more advanced surface evaluations such as the solid surface tension. This important parameter further quantifies the wetting properties of a solid material. The reinforcement used in this manuscript is α-cellulose, a hydrophilic polymer. Therefore, to enhance the adhesion, or interface between the resin and fiber, it is vital for the respective resin to contain hydrophilic regions. These hydrophilic regions ensure favorable interactions and hydrogen bonding between the resin and fiber. Theoretically, enhancements to the resin-reinforcement interface, will lead to enhancements in the respective polymer's thermo-mechanical properties.

Static and dynamic contact angles were measured to affirm the validity of the measured angles. Accurate contact angle measurements can be difficult to determine and variable between

users. Contact angle measurements were analyzed on a ramé-hart contact angle telescope-goniometer with an automated dispenser utilizing a direct measurement method of the tangent angle at the three-phase contact point on a sessile drop. The contact angle is determined from the angle of the tangent line formed from the liquid-solid surface to the liquid-vapor interface. The three-phase contact points refers to the interphase where liquid, solid and vapor interact. The more favorable the interactions between the liquid and solid interphases, the lower the contact angle due to the increased width of liquid dispersion on polymer surface. Generally, angles less than 90° are favorable, while angles greater than 90° are considered unfavorable, and therefore, the liquid-solid interphase would be minimized.

For the static contact angle measurements 2 μL of water was dispensed onto a flat polymer surface and the contact angle was measured every 30 seconds for a total of 10 measurements, and repeated for a total of three trials. The average angle and standard deviations from the three trials were obtained and are listed in Table 7. Since the [ME] resin wasn't completely uncured and contained a significant amount of unreacted materials in comparison to the [TO] and [A], contact angle analyses were conducted on resins cured at 130°C for 24 hours. Based on the DSC analysis of the [ME] resin cured at 130°C for 24 hours, by increasing the reaction time an additional 6 hours, the polymerization went to completion, as evidence by the absence of any exothermic peaks (Figure 25). Resin [A] had the most favorable interactions with water, indicating an increase in hydrophilicity by replacing tung oil, a triglyceride, with its fatty acid, α-eleostearic acid. Despite the slight changes in molecular structure between the resins, the structure manipulation from an ester group to a carboxylic acid, as well as the decrease in steric hindrance from the removal of the triglyceride glycerol backbone, increased the flexibility and hydrophilicity of resin [A] to reorient its polar groups in response to the water interaction. Not

surprisingly, [ME] and [TO] resins had comparable results most likely attributed from their similar functional groups. Although, [ME] is more flexible than [TO] due to its absence of the glycerol backbone, therefore increasing the ability of the molecules to reorient its polar groups in response to the water. The hydrophobicity nature of the long carbon chain, and decreased hydrophilicity of the ester group in comparison to carboxylic acids, counteracts the [ME] flexibility, and the overall interaction with water is unfavorable.

Thermodynamic factors, heterogeneity surfaces, and surface roughness can affect the contact angle, making a single static angle reading inadequate for precise measurements. Therefore, a dynamic analysis is used for these measurements which accounts for the surface roughness and sample heterogeneity. During analysis, the contact angles are generated by slowly enlarging the droplet size, referred to as the advancing contact angle (θ_a), and then retracting the subsequent liquid, receding contact angle (θ_r). For each expanding or retraction step, 0.25 μL of liquid per measurement was used. After the initial drop's contact angle stabilized, the advancing angle was determined at the point when the angle was no longer increasing (at a difference greater than 0.5°-1°), but the drop width was still increasing with each additional step. While the receding angle (θ_r) was determined at the point during liquid retraction where the angle was continuous decreasing, but the width was no longer changing (a difference less 0.5). Calculations of the difference between the receding and advancing contact angles is known as the contact angle hysteresis. The numerical value of the hysteresis is an indication of how rough or heterogeneous the polymer surface is. Theoretically, if the hysteresis value is 0, then the experimentally obtained contact angle represents the Young's contact angle θ_Y. Young's contact angle is commonly used in advanced surface studies to calculate the surface tension. Regardless, in previous literature the advancing angle has shown to be a good approximation of Young's

contact angle.[67] While, consequently, the receding angle has been determined to less accurate because of polymer swelling or liquid absorption.[68]

Based on the data results in Table 7, a similar trend to that of the static contact angles was found. Despite the similarities, there was an increase in hydrophobicity found in the dynamic contact angles in all the polymers. This is most likely due to the polymer's ability to absorb water, yielding false angles in the static angles since the angles were taken over a 5-minute period. Amble time for some of the liquid to absorb. Resin [A] displays the highest value for hysteresis, which normally would be an indication that the polymer is the most heterogeneous or has a rough surface. Although the surface degree of roughness can not be ruled out for contributing to the high hysteresis value, the more likely explanation for the significant difference in the advancing and receding angles in resin [A] is because of the polymer's enhanced ability to absorb water in reference to the other polymers. This theory is further confirmed by water uptake/absorption studies (Table 8).

Resin	Static Angle	Receding Angle	Advancing Angle	Hysteresis
A	36.70	41.1	80.8	39.7
ME	100.77	106.6	121.4	14.8
TO	97.93	117.5	130.6	13.1

Table 7. Contact angle measured by goniometer of static and dynamic angles (Receding and Advancing angles). All resins were cured at 130°C for 24 hours.

Water uptake experiments were used to determine the polymer's ability to absorb water which consequently can be used to make inferences about its ability to biodegradable. As well as to provide some insight to the high standard deviation values found in the contact angle measurements. [TO], [A], and [ME] polymers cured at 130°C for 18 hours, were weighed at their

dry state (W_d), and then submerged in water for 24 hours. After 24 hours, the subsequent polymers (W_w) were weighed after the excess water was removed by a kimwipe. Equation 10 was used to calculate the respective percentage of water absorption/uptake. Resin [A] displayed a 90% water uptake value (Table 8). Indicating favorable interactions with water and a high potential for biodegradability. Resin [ME] also showed a significant amount of water uptake despite its hydrophobic nature, yielding exciting potential for biodegradability as well. [TO] resin only showed a 7% weight increase despites its equivalent hydrophobicity as [ME]. In comparison to [A] and [ME], [TO] is significantly more cross-linked, providing rigidity and stability to the polymer. Due to this high cross-linked network, the polymer can not swell or absorb water as easily as the other polymers. Although, the high cross-link density in [TO] provides good thermo-mechanical properties, it consequently is more difficult to degrade naturally. As with most thermosetting polymers, the [TO] polymer would have to undergo harsher conditions to be recycled.

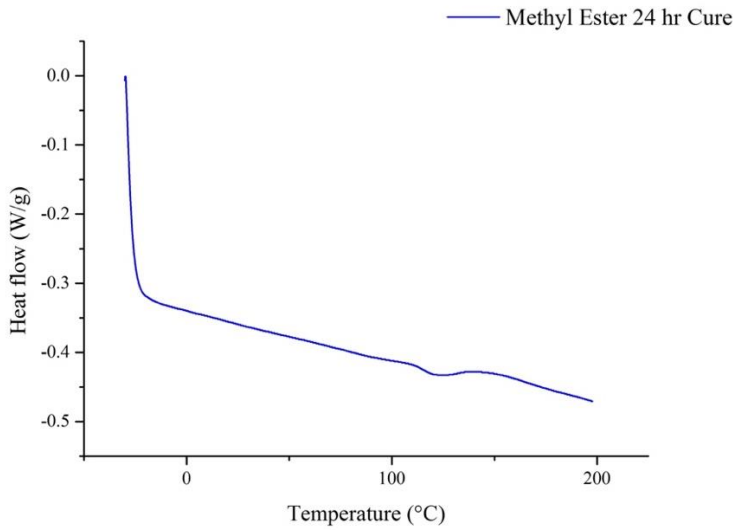

Figure 25. DSC analysis of the methyl ester [ME] resin cured at 130°C for 24 hours.

$$\text{Ratio} = \frac{W_w - W_d}{W_d} * 100 \quad (10)$$

Resin	Weight Wet (W_w)	Weight Dry (W_d)	Ratio
A	0.0448 g	0.0236 g	90%
ME	0.0395 g	0.0276 g	43%
TO	0.0412 g	0.0384 g	7%

Table 8. Resin water absorption ratios based on equation 10, cured at 130°C for 18 hours.

CHAPTER 4: CELLULOSE REINFORCED COMPOSITES

4.1 MATERIALS

α-cellulose powder, n-butyl methacrylate (BMA), di-tert-butyl peroxide (DTBP), and tung oil (TO), (DTBP) were brought from Sigma-Aldrich (St. Louis, MO). Divinylbenzene (DVB) was purchased from TCI America (Portland, OR). The resin-fiber interface analyses were completed on a JSM-760F Field Emission Scanning Electron Microscope (JEOL, Peabody, MA), using an accelerating voltage of 1.0 kV, and lower detector scanning mode (LEI). The dynamic mechanical analyses (DMA) were recorded on a TA Instruments Q800 dynamic mechanical analyzer (New Castle, DE) using a three-point bending mode. DMA experiments were conducted under the same experimental parameters as the resins (see section 3.1). The thermo-stability properties were conducted on a Q50 thermal gravimetric analysis (TGA) instrument (TA Instruments, New Castle, DE). The TGA was run under air from room temperature to 500°C at various heating rates.

4.2 COMPOSITE PREPARATION

Fatty acid composites were prepared by melting the desired amount of fatty acid based on its pre-determined composition ([A], [NN] or [Z]) in its respective amounts of co-polymers, DVB and BMA, in a 20 mL vial at 50°C. Once the sample was completely liquefied, the solution was vortexed for 30 seconds to ensure the production of a homogenous mixture. The solution was saturated with α-cellulose powder, equating to 3 g (23%), and was allowed to settle before 0.5 g of the free radical initiator, DTBP was added. The solution was vortexed again and placed in the convection oven at 130°C for 18 hours (Figure 25). Methyl ester and tung oil resins were prepared in an identical manner minus the initial melting step at 50°C. The tung oil and methyl

ester starting materials were directly added to the 20 mL vial, vortexed, and then followed the previous composite preparation steps.

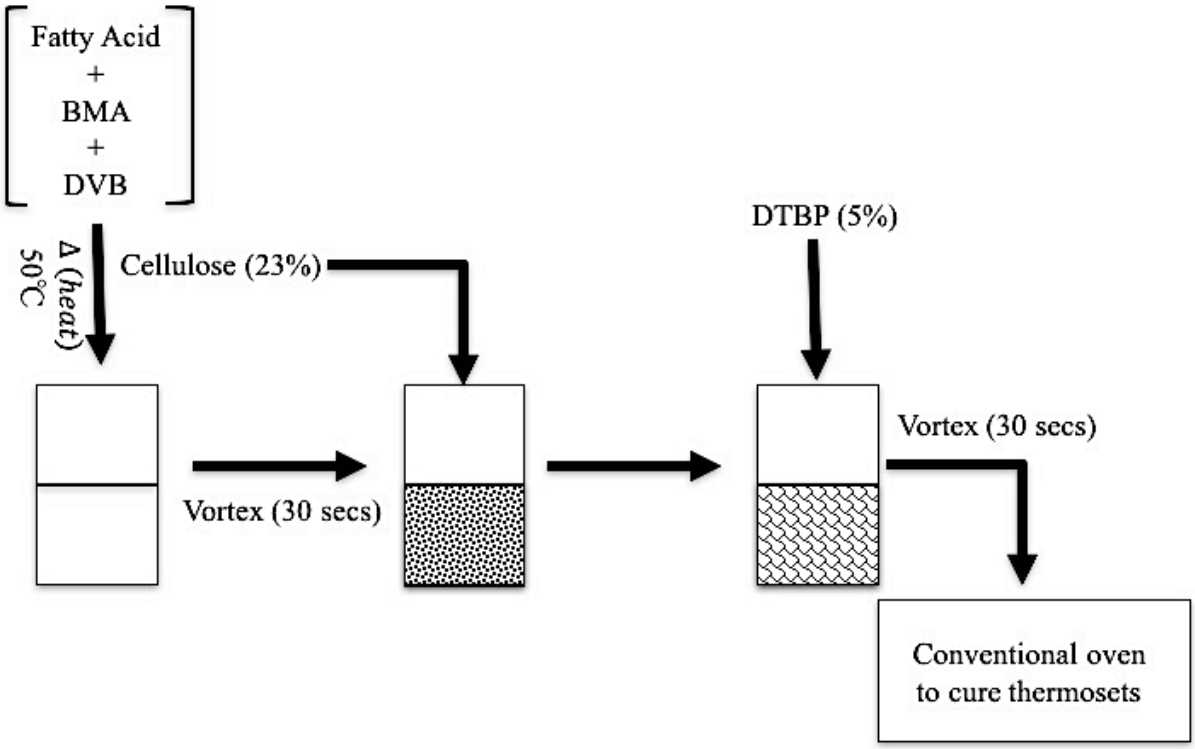

Figure 26. General schematic of the composite sample preparation cured in a convection oven.

4.3 FIBER-RESIN ANALYSIS VIA SCANNING ELECTRON MICROSCOPE

Fatty acid [A+C], tung oil [TO+C] and methyl ester [ME+C] composites were analyzed under SEM using an accelerating voltage of 1.0 kV, and lower detector scanning mode (LEI) at 2000 (TO and FA) and 2500 (ME) magnifications. Based on the SEM images (Figure 27), the cellulose fiber is adhering well with the resin in the [A+C] composite (Figure 27A), as indicated by the resin residue on the fiber. In the methyl ester composite [ME+C], the fiber is not interacting with or adhering to the resin, as indicated by the lack of resin residue on the fiber (Figure 27B). Also, there is a clear distinction between the fiber and resin, as illustrated by the shadow casted from the fiber onto the resin. The tung oil [TO+C] composite (Figure 27C) displays some adhesion between the resin and fiber, despite its hydrophobic nature. The

perceived enhanced adhesion with cellulose, in comparison to [ME+C], is inherited from the tung oil polymer's rigidity and high cross link density. Therefore, due to the polymer's constrictive nature, the unfavorable interactions between the fiber and resin can not segregate the resin and fiber. In which case, the interactions between cellulose and the [TO] resin are not due to polarity, but to the high cross-link density within the resin and entrapment of the fibers. [ME+C] is very flexible, and thus, has a low cross-link density, as discussed in the following mechanical properties section 4.4. This decrease in rigidity because of the polymer's low reactivity and oligomer chains that are acting as plasticizers between cross-linked chain. These incorporated chains allow for the fibers and resin to segregate because their molecular mobility is not hindered by cross linking. Overall, the [A+C] showed the most promising adhesion properties with the reinforcement, cellulose. Due to the hydrophilicity nature of the [A] resin based on the contact angle results discussed in the previous section, it is not surprising that it adhered the best to cellulose.

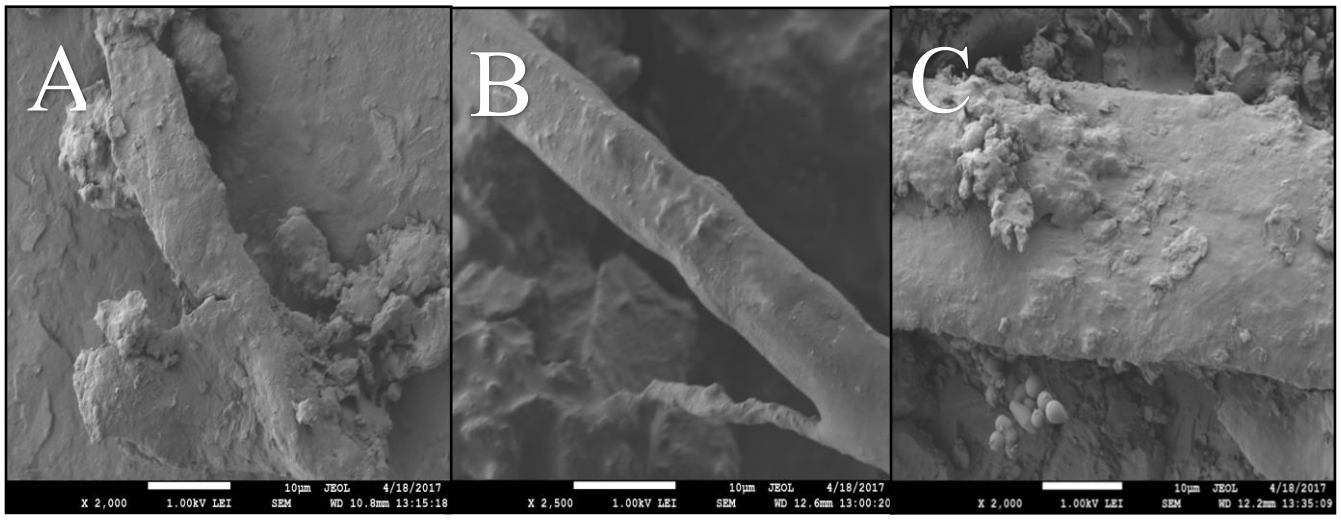

Figure 27. SEM images coated with gold of resin-fiber interfaces of **(A)** fatty acid composite [A], **(B)** methyl ester composite [A], and **(C)** tung oil composite [A] cured at 130°C for 18 hours.

4.4 COMPOSITE MECHANICAL PROPERTIES

The composites' mechanical properties were analyzed by DMA in a multi-frequency-strain mode, using the three-point bending clamp from -60°C to 150°C. Similar degradation trends as in the resins discussed in section 3.4, were found. These composites display the characteristics of the three distinct viscoelastic regions: the glassy state, glass transition state, and rubbery plateau state. Although, unlike the resins, the composites display distinct differences in storage modulus at throughout the DMA analyses. The fatty acid based composites ([NN+C], [A+C], and [Z+C]) displayed similar mechanical properties in their glass states until around $-10°C$, where they are beginning to transition into glass transition states. The early onset of segmental relaxation in comparison to the resin onset (0°C), is most likely due to the addition of cellulose which is less thermally stable than the resins. Regardless of the viscoelastic state, [TO+C] had the highest storage modulus of all the composites. As expected and shown in the resin DMA analysis, the composites' storage modulus decreases as the temperature increases. From around 0°C to 75°C, there is a sharp decrease in the storage modulus as the composites are transitioning from their brittle, rigid states to their more fluid, glass transition states, and ultimately above their respective T_gs. From around 75°C to end experimental temperature, 150°C, the composites' storage modulus plateaus as it reaches into the rubbery plateau region. This region is indicative of cross-linked polymers. Before this region, the polymer's stiffness had been decreasing with the increasing temperature, due to the increase mobility and resulting fluidity of the structure. The cross-link network provides a rigid structure that can no longer flow past a certain point, rubbery plateau, due to steric hindrance despite the temperature increase. Therefore, the E', and resulting stiffness or elasticity of the polymer is no longer changing until the temperature is increased enough for sample degradation.

Based on the results from Figure 28 and Table 9, the composite [ME+C] showed the weakest mechanical properties, a similar trend that the resin displayed, since it was too brittle to even be tested. [TO+C] displayed the best mechanical properties, as expected, due to the enhanced mechanical properties the resin [TO] displayed in comparison to the other polymers. As the DVB weight percentage increased in the fatty acid based composites, the storage modulus increased. It is no coincidence that the mechanical property trends between the resins and composites are similar, if not identical. Cellulose is used as reinforcement to enhance the mechanical properties of the resins. The pre-existing trends based on the monomer composition are not significantly changed by the addition of cellulose. Additionally, the composites do not exhibit secondary relaxations in the E' curves, and therefore, indicate a single T_g range and a homogenous mixture.

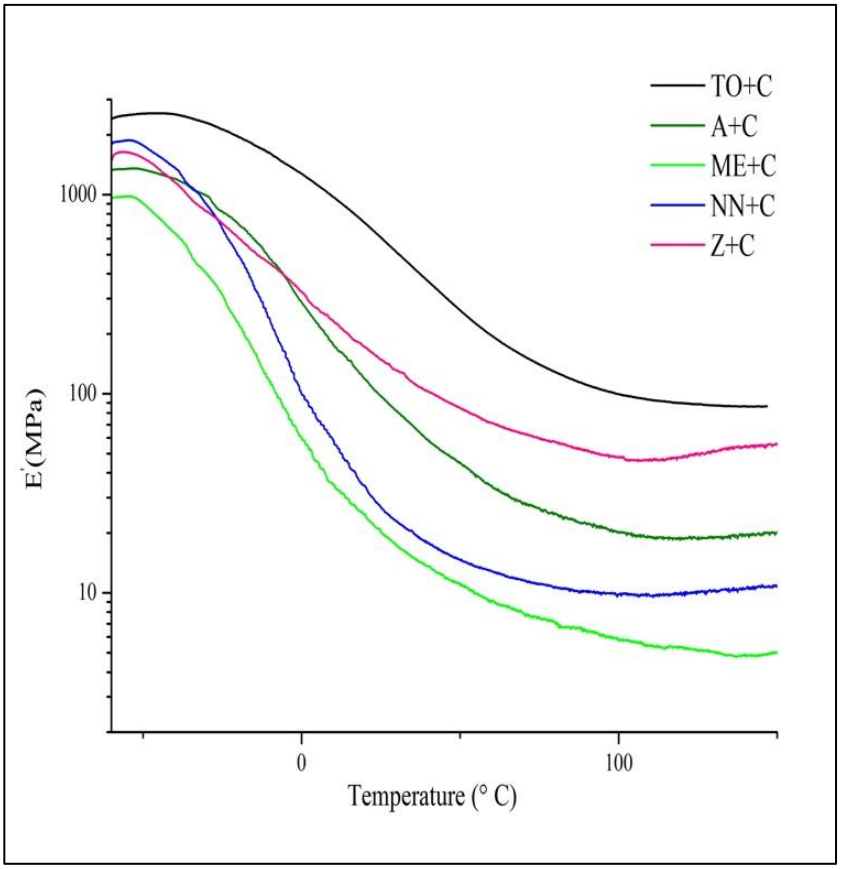

Figure 28. DMA storage modulus, E' curves of composites

Based on the tan δ curves (Figure 28) [NN+C] has the best damping properties, followed by the [ME+C] composite. Between the composites and resins evaluations, the width of the tan δ curves did not significantly change. Which indicates that the addition of cellulose did not disrupt the heterogeneity or homogeneity nature of the polymers. Also, indicating that cellulose fibers have been distributed throughout the polymer, providing universal thermo-mechanical properties for the entire sample. The maximum value of the tan δ curve represents the glass transition temperature (T_g) (Figure 29). [ME+C] had the lowest T_g. Due to its poor adhesion between the resin and reinforcement, the composite was able to flow more freely at a lower temperature than the other composites. [A+C] and [Z+C] fatty acid based composites, saw an increase in T_g in comparison to their respective resins. These enhancements in thermo-mechanical properties, are most likely due to the increase in compatibility between the resin and reinforcement fiber. The [NN+C] composite, despite its theoretical increase in compatibility, did not show an increase in T_g. It is possible that the low cross link density within the polymer is the main contributing factor to why there was not an enhancement in thermo-mechanical properties. The [A+C] composite, and especially [Z+C] composite, are significantly more cross-linked than [NN+C]. The compatibility between cellulose and resin in the fatty acid polymers, in addition to the cross-link density, could be working in a synergistic manner, therefore increasing the thermo-mechanical properties. Despite the lack of increase in [NN+C] and [TO+C] thermo-mechanical properties (T_gs), the composites did have substantial increases in mechanical properties based on the storage modulus (Figure 28).

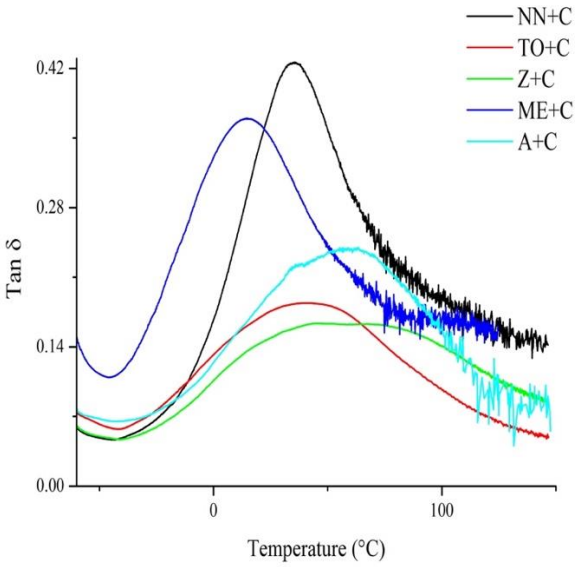

Figure 29. Composite tan δ curves from DMA

	FA (g)	DVB (g)	BMA (g)	Cellulose (g)	Glass Transition (℃)[a]	Storage Modulus E' (25℃)[b]	Storage Modulus E' (T_g + 50℃)[c]
NN+C	4.5	1.0	4.5	3.0	28℃	288.2 MPa	21.19 MPa
A+C	5.0	2.0	3.0	3.0	56℃	459.5 MPa	31.66 MPa
Z+C	6.0	3.5	0.5	3.0	68℃	994.9 MPa	120.0 MPa
ME+C*	5.0	2.0	3.0	3.0	15℃	20.40 MPa	8.573
TO+C**	5.0	2.0	3.0	3.0	32℃	524.0 MPa	131.2 MPa

Table 9. [a] Glass transition temperatures evaluated from the tan δ curves, [b,c] storage modulus from the E' curves, evaluated from the DMA analyses of tung oil (TO), fatty acid composition [A] (A), fatty acid composition [NN] (NN), and fatty acid composition [Z] (Z) resins. *Methyl ester based composite. ** Tung oil based composite.

4.5 COMPOSITE THERMO-STABILITY PROPERTIES

For comparison purposes the composites' thermal properties evaluated by the identical experimental TGA parameters as the resins. The composites were run under air from room

temperature to 500°C at various heating rates (2°C/min, 5°C/min, 10°C/min, or 20°C/min). At low temperatures, below 100°C, all the composites are thermally stable, and there are only subtle differences in their thermal properties (Table 10). Cellulose is less thermally stable than the resins and well known for absorbing water. From around room temperature to 100°C, the weight loss is contributed to the evaporation of water in cellulose and the composites (Figure 30). As in the resins, the composites exhibit characteristics of a multi-stage degradation. As previously mentioned, from around room temperature to 100°C water is being evaporated in the composites. The next degradation stage is from around 100°C to 300°C and represents the evaporation of soluble, unreacted materials, as well as their respective decomposition. As well the early stages of the cellulose and resin degradation. From around 300°C until 450°C is the region with the fastest degradation, suggested by the steepest slope. In this region, the cross-link network is rapidly degrading as the composite is becoming charred. Although the rate of degradation and overall thermal stability is highly dependent on the polymer composition as shown in Figure 30.

In the beginning stages of degradation, the composites with the highest cross-link densities are the most thermally stable. As expected, since cellulose is generally less stable than the resins and therefore, the stability arises from the resins composition. Although, [Z+C] initially displays the best thermo-properties, which could be due to the increased hydrogen bonding potential with cellulose from the increased percentage of fatty acid. The superiority thermal stability quickly fades in the later stages of degradation. At which point, the resin composition and cross-link densities determine the thermal stability. Once degradation started, [TO+C] displayed the best thermo-properties until T_{75}. At this point, the composites have become char and no longer have the same molecular structure. [ME+C] showed the worst thermo-properties, after the initial stages of degradation. Most of the other composites

maintained their cross-link network structure until around 300°C, but [ME+C] started its fastest degradation at around 200°C. Overall, the superiority of the composites' thermo-properties is as follows: [TO+C] > [Z+C] > [A+C] > [NN+C] > [ME+C].

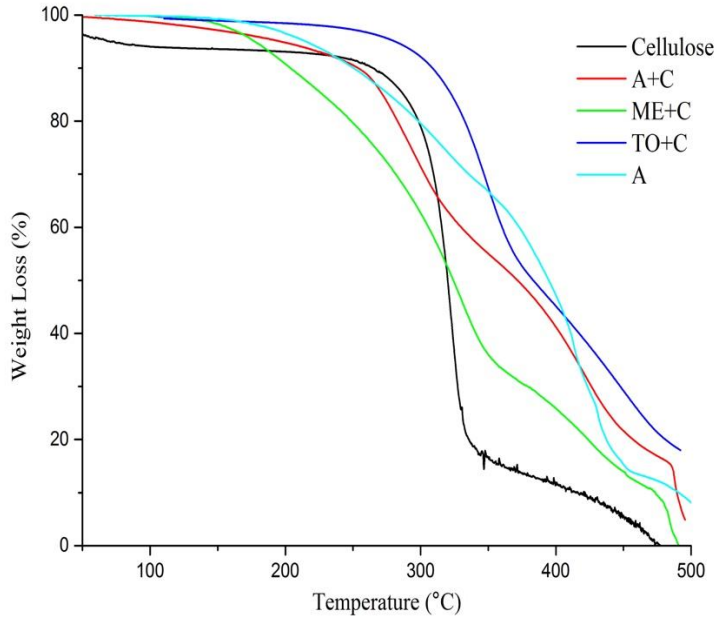

Figure 30. Thermal degradation of composites analyzed by TGA, and run under air from room temperature to 500°C at a heating rate of 10°C/min.

	T_{start} (℃)[a]	T_{10} (℃)[b]	T_{20} (℃)[c]	T_{50} (℃)[d]	T_{75} (℃)[e]
NN+C*	90.0	238.4	286.46	343.80	450.08
A+C*	106.01	254.04	282.92	370.85	438.55
Z+C*	130.68	263.41	295.06	432.30	491.95
ME+C	101.54	203.42	248.04	323.88	403.91
TO+C	101.29	304.37	329.74	382.92	462.40
Cellulose	26.64	264.19	298.14	319.93	330.95

Table 10. Cellulose and composites thermal degradation temperatures at the [a] start of degradation, 0.5%, [b] 10% weight loss, [c] 20% weight loss, [d] 50% weight loss, and [e] 75% weight

loss extracted from TGA curves run under air at a heating rate of 10°C/min. *Fatty acid based composite.

4.5.1 COMPOSITE DEGRADATION ACTIVATION ENERGY

The degradation activation energy was determined by equations 2-9 found in section 3.5.1, as well as the same procedure for deriving the isoconversional points and the resulting activation energy. Similar trends were found as in the TGA curves. The composites have a lower degradation activation energy than the resins. As previously mentioned, this is because cellulose is less thermally stable than the resins. Therefore, by combining the two compounds, a composite with properties found in the middle is formed. Theoretically, this phenomenon makes sense as well. Hydrogen bonds are much easier to break than covalent bonds, and therefore, by nature the composites are less stable than the resins. The [TO+C] composite was found to have the highest degradation activation energy, correlating to the most thermally stable. At 5% weight loss, the methyl ester composite seems to have a higher degradation activation energy than the fatty acid composite. Although, based on the previously discussed DSC curves, [ME] is not fully cured. Therefore, at low weight loss percentages, consequently corresponding to lower temperatures, the [ME+C] is undergoing a polymerization reaction. This trend was also found in the resins degradation activation energy, but the [ME] stability superiority to the fatty acid resin was not. The misleading superiority is only found present in the composites because of the lowered stability through the addition of cellulose. The fatty acid composite stability is affected more than the methyl ester composite, because the fatty acid composite is completely cured. Therefore, in terms of the composites' thermal stability, the 10% and 20% weight loss are more representative of the degradation activation energy.

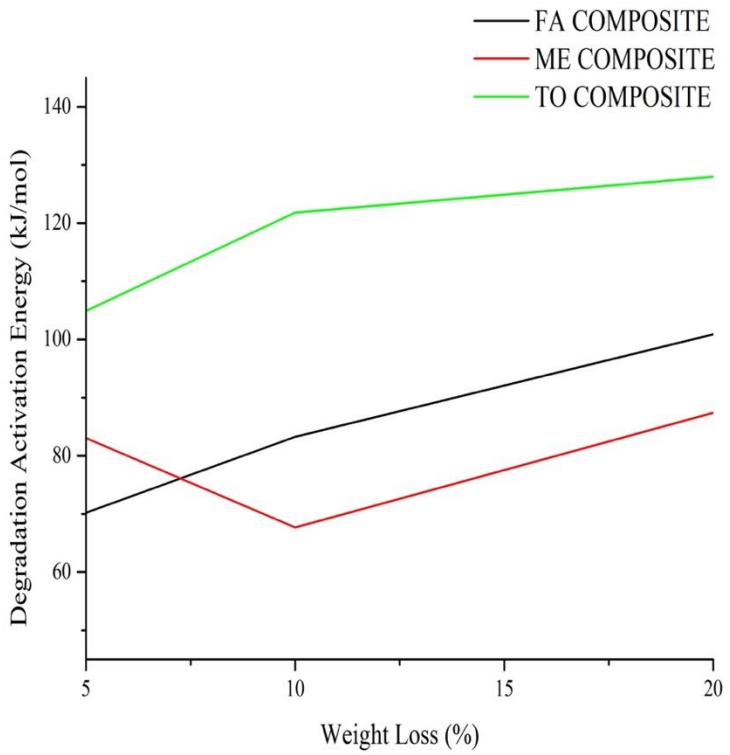

Figure 31. Composite degradation activation energy.

Sample	Weight Loss (%)	Activation Energy (kJ/mol)
FA Composite	20	100.87
	10	83.23
	5	70.19
TO Composite	20	127.94
	10	121.79
	5	104.88
ME Composite	20	87.41
	10	67.67
	5	83.03

Table 11. Composite degradation activation energy raw data.

CHAPTER 5: CONCLUSIONS

In conclusion, this thesis discusses the successful extraction and isolation of the fatty acid, α-eleostearic acid, and its corresponding polymerization in efforts to enhance the resin-reinforcement interface. The resulting enhancement in compatibility between the resin and reinforcement should consequently lead to better thermo-mechanical properties in the bio-based composites. Comparison studies between fatty acid, methyl ester and tung oil were completed to examine the effects of thermo-mechanical properties based on the structural chemical modifications of the starting materials.

The fatty acid was extracted by a simple saponification reaction and does not produce harmful waste products resulting in an overall environmentally friendly and renewable material. The successful extraction and isolation of the fatty acid was analyzed by Raman, FT-IR, GC-MS and ^{1}H NMR (Chapter 2).

To enhance the thermomechanical properties, α-eleostearic acid was co-polymerized with two co-monomers, butyl methacrylate (BMA) and divinylbenzene (DVB) and cured in a programmable convection oven. The free radical polymerization of the resins was monitored by dielectric analysis (DEA), differential scanning calorimetry (DSC) and Raman spectrometry (Raman) to obtain the optimal cure schedule. The morphology of the resins was examined by scanning electron microscopy (SEM) and resin composition [A] was determined to be the best combination of monomers (50% FA, 20% DVB, and 30% BMA). The hydrophilicity of the resins was measured by contact angle goniometer (contact angle), and water uptake/absorption analyses. Resin [A] had the most favorable interactions with water based on these analyses, implying that resin [A] was the most hydrophilic. As well the most promising resin for natural decomposition. The thermo-mechanical properties of the newly cured resins were analyzed by

thermogravimetric analysis (TGA), and dynamic mechanical analysis (DMA). Resin [TO] had the best thermo-mechanical properties due to its rigid triglyceride structure, and glycerol backbone. Overall, the resins showed an increase in mechanical properties as the DVB content increased. The methyl ester resin displayed the worst thermo-mechanical properties, as expected based on its poor reactivity with the co-polymers (Chapter 3).

Once the optimal cure schedule was determined, the resins were reinforced with cellulose fibers to enhance the thermo-mechanical properties (Chapter 4). The resin-reinforcement binding was analyzed under scanning electron microscopy (SEM). Composite [A+C] had the best binding with cellulose based on SEM. The thermo-mechanical properties of the composites were studied by thermogravimetric analysis (TGA), and dynamic mechanical analysis (DMA). Despite the better binding with cellulose, [A+C] does not have the thermo-mechanical strength that [TO+C] does. Similar DVB trends were found in the fatty acid composites as presented in the resins. Overall, [ME+C] had the most inferior thermo-mechanical properties.

To the best of our knowledge, this fatty acid based polymer has not been made before and would be a novel contribution to the scientific community. When applicable, the fatty acid based composite should be used over the other composites in terms of recyclability, based on resin [A]'s enhanced ability to absorb water, and overall superior thermo-mechanical properties in reference to the methyl ester resin and composite. However, if the application requires high thermo-mechanical strength, disregarding recyclability and wettability, then the tung oil composite would be the appropriate polymer of choice; and has been frequently utilized in previous research. Overall, this research provides viable and promising initial research regarding the enhancement of resin-reinforcement compatibility. Research which can be used for future

experiments contributing to the global goal of engineering bio-based polymers that are biorenewable and eco-friendly.

SUPPLEMENTAL DATA

	FA (g)	DVB (g)	BMA (g)	Testable	Result		
	1	1	8				
	2	1	7				
ii	3	1	6	-	too many cracks		
hh	4	1	5	-	too many cracks		
NN	4.5	1	4.5	+	softer than OO and less cracks		
O	5	1	4	-	too soft		
N	6	1	3	-	too soft		
L	7	1	2	-	too soft; liquidly and very sticky		
	7.5	1	1.5		same DVB/BMA ratio as A		
	1	1.5	7.5				
	2	1.5	6.5				potential with alternated hardness
kk	3	1.5	5.5	-			
jj	4	1.5	4.5	-			failed
OO	4.5	1.5	4	+/-	harder than NN but more cracks		
P	5	1.5	3.5	-	too soft but no cracks		
K	6	1.5	2.5	-	too soft but no cracks		avoiding based on previous results
	7	1.5	1.5				
R	1	2	7	-	Too brittle, a lot of cracks		DMA graphs completed
S	2	2	6	-	Too brittle, a lot of cracks		
T	3	2	5	-	Too brittle, a lot of cracks		best sample
E/U	4	2	4	-	Too brittle, a lot of cracks		
ll	4.5	2	3.5	-			
A	5	2	3	+	Very little cracks		
ff	5.5	2	2.5	+/-	cracks; maybe get a good sample		
Q	6	2	2	+/-	soft but has potential		

M	7	2	1	-	too soft
	1	2.5	6.5		
	2	2.5	5.5		
	3	2.5	4.5		
J	4	2.5	3.5	-	too many cracks
W	5	2.5	2.5	-	too many cracks
mm	5.5	2.5	2	+/-	cracks; maybe get a good sample
i	6	2.5	1.5	+	some cracks
ee	6.5	2.5	1	+/-	cracks; maybe get a good sample
V	7	2.5	0.5	-	too soft but no cracks
pp	2.5	3	4.5	-	same DVB/BMA ratio as A
D	3	3	4		
B	4	3	3	-	too many cracks
G	5	3	2	-	too many cracks
X	6	3	1	-	too many cracks
QQ	6.5	3	0.5	-	too many cracks and fractured on impact
	1	3.5	5.5		
	2	3.5	4.5		
	3	3.5	3.5		
H	4	3.5	2.5	-	too many cracks
Y	5	3.5	1.5	-	too many cracks
gg	5.5	3.5	1	-	
Z	6	3.5	0.5	+	some internal cracks
	1	4	5		
	2	4	4		
C	3	4	3		
aa	4	4	2	-	too many cracks
bb	5	4	1	-	too many cracks
	1	4.5	4.5		
	2	4.5	3.5		
	3	4.5	2.5		
	4	4.5	1.5		
cc	5	4.5	0.5	-	too many cracks
	1	5	4		
	2	5	3		
	3	5	2		

dd	4	5	1	-	too many cracks
	1	5.5	3.5		
	2	5.5	2.5		
	3	5.5	1.5		
	4	5.5	0.5		
	1	6	3		
	2	6	2		
	3	6	1		
	1	6.5	2.5		
	2	6.5	1.5		
	3	6.5	0.5		
	1	7	2		
	2	7	1		
	1	7.5	1.5		
	2	7.5	0.5		
	1	8	1		

Table 2. Fatty acid (FA), divinylbenzene (DVB), and butyl methacrylate (BMA) monomer combinations in polymers cured at 130°C for 18 hours.

REFERENCES

[1] Yuan, H.; Yang, B.; Zhu, G. "Biodiesel Production with Water-Tolerance and Microwave Absorbing Catalyst Using Tung Oil." International Journal of Green Energy 10.10 (2013): 999-1010.
[2] Belyi, A.,V. "Why is the oil price not about equilibrium?: An economic sociology account of petroleum markets." Energy Policy. 96, 45-49, Sept. 1, 2016.
[3] Mosiewicki, M., et al. "Moisture Dependence of the Properties of Composites Made from Tung Oil Based Polyurethane and Wood Flour." Journal of Polymer Research 19.2 (2012): 1-8.
[4] Salimon, J.; Abdullah, B. M.; Salih., N. "Saponification of Jatropha curcas Seed oil: Optimization by D-Optimal Design." International Journal of Chemical Engineering. (2012). *2012,* 1-6.
[5] Belgacem, M.N.; Gandini, A. Materials from vegetable oils: major sources, properties and applications. In: Belgacem MN, Gandini A, editors. Monomers, polymers and composites from renewable resources. Amsterdam: Elsevier Ltd; 2008. p. 17–39.
[6] Faruk, O.; Bledzki, A.K.; Fink, H.P.; Sain, M. "Progress report on natural fiber reinforced composites." Macromol Mater Eng 2014; 299:9–26.
[7] Chengguo, Liu, et al. "Tung Oil Based Monomer for Thermosetting Polymers: Synthesis, Characterization, and Copolymerization with Styrene." Bioresources 7.1 (2012): 447-463.
[8] Wool, R., ln: Wool, R.P., Sun, X.S., editors. Polymers and composite resins from plant oils in bio-based polymers ad composites, Burlington (USA); Elsevier Academic Press; 2005.p.56-113.
[9] Lu, Y.S.; Larock, R.C. (2009) "Novel polymeric materials from vegetable oils and vinyl monomers: preparation, properties, and applications." ChemSusChem 2:136-147.
[10] Xia,Y.; Larock, R.C. (2010) "Vegetable oil-based polymeric materials: synthesis, properties, and applications." Green Chem 12:1893-1909.
[11] Khot, S.N.; Lascala, J.J.; Can, E.; Morye, S.S.; Williams, G.I.; Palmese, G.R.; et al. "Development and application of triglyceride-based polymers and composites." J. Appl Polym Sci, 82 (2001), pp. 703–723.
[12] Schönemann, A.; Frenzel, W.; Unger, A.; Kenndler, E. (2006). "An Investigation of the Fatty Acid Composition of New and Aged Tung Oil." Studies in Conservation, 51(2), 99-110.
[13] Bisio, A.; Xanathos, M. How to manage plastics waste. (1995). Hanser. Munich, New York, USA.
[14] Mustafa, M. Plastic Waste Management: Disposal, Recycling, Reuse. (1993). Marcel Dekker, New York, USA.
[15] Frederick, T.; Wallenberger, T.; Norman, E., editors. Natural Fibers, plastics and composites, Boston (USA); Kluwer Academic Publishers, 2004.
Springer, 2004.
[16] Kaufman, M.; Wiesman, Z. "Pomegranate Oil Analysis with Emphasis on MALDI-TOF/MS Triacylglycerol Fingerprinting." Journal of Agricultural and Food Chemistry. (2007). *55*, 10405-10413.
[17] Liu, C.; Yang, X.; Cui, J.; Zhou, Y.; Hu, L.; Zhang, M.; Liu, H. "Tung Oil Based Monomer for Thermosetting Polymers: Synthesis, Characterization, and Copolymerization with Styrene."Bioresources 7.1 (2012): 447-463.

[18] Pfister, D. P.; Baker, J. R.; Henna, P. H.; Lu, Y.; Larock, R. C. (2008). "Preparation and properties of tung oil-based composites using spent germ as a natural filler." Journal of Applied Polymer Science, 108(6), 3618.
[19] Meiorin, C.; Mosiewicki, M.A.; Aranguren, M.I. "Ageing of thermosets based on tung oil/styrene/ divinylbenzene." Polymer Testing 32 (2013) 249–255
[20] Mosiewicki, M.A.; Rojas, O.; Sibaja, M.R.; Borrajo, J.; Aranguren, M.I. "Aging study of linseed oil resin/styrene thermosets and their composites with wood flour." Polym. Int. 56 (7) (2007) 875–881.
[21] Larock, R. C.; Li, F. "Thermosetting Polymers from Cationic Copolymerization of Tung Oil: Synthesis and Characterization." J. Appl. Polym. Sci. (2000). 78, 1044.
[22] Li, F.; Hanson, M. V.; Larock, R. C. "Soybean oil–divinylbenzene thermosetting polymers: synthesis, structure, properties and their relationships." Polymer. (2001). 42, 1567.
[23] Hondred, P.; R., Salat, L.; Mangler, J.; Kessler., M. R. "Tung Oil-Based Thermosetting Polymers for Self-Healing Application." Journal of Applied Polymer Science. (2014). *131*, 40406.
[24] Montero de Espinosa, L.; Meier, M.A. (2011). "Feature Article: Plant oils: The perfect renewable resource for polymer science?!." European Polymer Journal, 47837-852
[25] Mosiewicki, M.A.; Casado, U.; Marcovich, N.E.; Aranguren, M.I. "Polyurethanes from Tung Oil: Polymer Characterization and Composites." Polymer Engineering and Science. (2009).
[26] Ashraf, S. M.; Ahmad, S.; Riaz, U. (2007). "Development of novel conducting composites of linseed-oil-based poly(urethane amide) with nanostructured poly(1-naphthylamine)." Polymer International, 56(9), 1173-1181
[27] Sharma, H. O.; Alam, M.; Riaz, U.; Ahmad, S.; Ashraf, S. M. (2007). "Miscibility Studies of Polyester amides of Linseed Oil and Dehydrated Castor Oil with Poly(vinyl alcohol)." International Journal of Polymeric Materials, 56(4), 437.
[28] Zhan, M.; Wool, R.P. (2010). "Biobased composite resins design for electronic materials." Journal of Applied Polymer Science, 118(6), 3274.
[29] Biermann, U.; Butte, Q.; Holtgrefe, R.; Feder, W.; Metzger, J.O. "Esters of calendula oil and tung oil as reactive diluents for alkyd resins." Eur. J. Lipid Sci. Technol. (2010). *112*. 103-109.
[30] Zheng, Y. Evaluation of Tung Oil Based Reactive Diluents for ALKYD Coating Using Experimental Design. 2014.
[31] Mosiewicki, M.A.; Casado, U.; Marcovich, N.E.; Aranguren, M.I. "Polyurethanes from tung oil: polymer characterization and composites." Polym Eng Sci 2009; 49: pp. 685–92.
[32] Haq, M.; Burgueño, R.; Mohanty, A.K.; Misra, M. "Bio-based unsaturated polyester/layered silicate nanocomposites: Characterization and thermo-physical properties." Composites Part A 2009a; 40: 540–547.
[33] Zhang, G.; Zhao, L.; Hu, S.; Gan, W.; Yu, Y.; Tang, X. "A Novel Biobased Resin-Epoxidized Soybean Oil Modified Cyanate Ester." Polym. Eng. Sci. 2008, 48, 1322.
[34]. Blaker, J.J.; Lee, K.Y.; Bismarck, A. "Hierarchical Composites Made Entirely from Renewable Resources." J. Biobased Mater. Bioenergy 5 (2011) 1–16.
[35] Quirino, R. L.; Larock, R. C. "Rice hull biocomposites, part 2: Effect of the resin composition on the properties of the composite." J. Appl. Polym. Sci. (2011). *121*, 2050.
[36] Quirino, R. L.; Woodford, J.; Larock, R. C. "Soybean and linseed oil-based composites reinforced with wood flour and wood fibers." J. Appl. Polym. Sci. (2012). *124*, 1520.

[37] Nozawa, A.; Nanamiya, H.; Tozawa, Y. "Production of membrane proteins through the wheat-germ cell-free technology." Methods in Molecular Biology (Clifton, N.J.). United States, 607, 213-218, 2010. ISSN: 1940-6029.
[38] Park, K.; Berrier, C.; Lebaupain, F.; Pucci, B.; Popot, J.; Ghazi, A.; Zito, F. (2007). "Fluorinated and hemifluorinated surfactants as alternatives to detergents for membrane protein cell-free synthesis." The Biochemical Journal, 403(1), 183-187.
[39] Johns, A.; Morris, S.; Edwards, K.; Quirino, R.L. "Asolectin from soybeans as a natural compatibilizer for cellulose-reinforced biocomposites from tung oil." Journal of Applied Polymer Science. (2015). *132*, 41833.
[40] Can, E.; Wool, R. P.; Küsefoğlu, S. "Soybean- and castor-oil-based thermosetting." J. Appl. Polym. Sci. 2006, 102, 1497-1504.
[41] Petrovic, Z.S.; Zhang, W.; Javni, I. "Structure and properties of polyurethanes prepared from triglyceride polyols by ozonolysis." Biomacromolecules 2005, 6, 713-719
[42] Petrovic, Z.S.; Guo, A.; Javni, I.; Cvetkonic, I.; Hong, D.P. "Polyurethane networks from polyols obtained by hydroformylation of soybean oil." Polym. Int. 2008, 57, 275-281.
[43] Andjelkovic, D. D.; Larock, R. C. (2006). "Novel rubbers from cationic copolymerization of soybean oils and dicyclopentadiene. 1. Synthesis and characterization." Biomacromolecules. 7, 927-936.
[44] Xia, Y.; Henna, P. H.; Larock, R. C. (2009). "Novel thermosets from the cationic copolymerization of modified linseed oils and dicyclopentadiene." Macromol. Mat. Eng. 294, 590.
[45] Johns, A.; Edwards, K.; Inglesby, S.; Quirino, R.L. (2016). "Emulsion Polymerization of Tung Oil-Based Latexes with Asolectin as a Biorenewable Surfactant." Coatings, Vol 6, Iss 4, P 56 (2016), (4), 56.
[46] Smith, M.; Payne, A.; Edwards, K.; Morris, S.; Beckler, B.; Quirino, R.L. "Effect of Microwave Cure on the Thermo-Mechanical Properties of Tung Oil-Based/Carbon Nanotube Composites." (2015). Coatings. 5(3), 557-575.
[47] Quirino, R.L.; Silva, T. F.; Payne, A.; Lopes, R.V.; Paterno, L.G.; Sales, M.J. "Synthesis and Thermomechanical Properties of Polyurethanes and Biocomposites Derived from Macauba Oil and Coconut Husk Fibers." (2015). Coatings. 5(3), 527-544.
[48] Gibbons, L.; Smith, M.; Quirino, R.L. (2015). "Modified lignin for composite and pellet binder applications." Int. J. Experimental and Computational Biomechanics, Vol. 3, pp. 200-214
[49] Young, R.J., and Lovell, P.A. *Introduction to Polymers*, 3rd ed.; CRC Press: Boca Raton, FL, 2011.
[50] Klemm, D.; Heublein, B.; Fink, H.; Bohn, A. (2005). "Cellulose: Fascinating Biopolymer and Sustainable Raw Material." Angew. Chem. Int. Ed. *44*, 3358.
[51] Quirino, R. L.; Silva, T. F.; Payne, A.; Lopes, R. V.V.; Sales, M. J. A. "Polyurethanes and Biocomposites Derived from Macauba Oil and Coconut Husk Fibers: Synthesis and Characterization." *Coatings*, v. 5, p. 527-544, 2015.
[52] Rodrigues, J. D. O.; Murawski, A.; Beckler, B.; Lopes, R. V. V.; Paterno, L. G.; Quirino, R. L.; Sales, M. J. A. Bio-based polyurethanes and composites from passion fruit oil methyl esters and coconut husk fibers; in *Biocomposites: Properties, Applications and Performance*, Shahzad, A. ed, NOVA publishers, Hauppauge, NY, USA, *in press.*
[53] Prakash, J.; Sokolsky, M.; Kumar, N.; Domb, A. J. (2008). Fatty Acid Based Biodegradable Polymer. Polymer Reviews, 48(1), 156-191.

[54] Hartmann, R. M.; Garzón, N. N.; Hartmann, E. M.; Oliveira, A. M.; Bazzo, E. (2013). "Vegetable Oils of Soybean, Sunflower and Tung as Alternative Fuels for Compression Ignition Engines." International Journal of Thermodynamics, 16(2), 87-96.
[55] Yang, X.; Zhang, S.; Li, W. (2015). "The performance of biodegradable tung oil coatings." Progress in Organic Coatings, 85:216-220
[56] The Editors of Encyclopædia Britannica. July 07, 2015. Ester. Encyclopædia Britannica, Inc.
[57] Quirino, R.L.; Larock, R.P. (2012). "Rh-based Biphasic Isomerization of Carbon-Carbon Double Bonds in Natural Oils." Journal of The American Oil Chemists' Society (JAOCS), 89(6), 1113-1124.
[58] Schönemann, A.; Edwards, H. M. (2011). "Raman and FTIR microspectroscopic study of the alteration of Chinese tung oil and related drying oils during ageing." Analytical & Bioanalytical Chemistry, 400(4), 1173.
[59] Thakur Vijay, K. Green Composites from Natural Resources. Taylor & Francis, 2014
[60] Lee, H.L. The Handbook of Dielectric Analysis and Cure Monitoring. 2014. Lambient Technologies. Boston, MA, USA.
[61] Mantheni, D.; Maheswaram, M.; Munigeti, R.; Perera, I.; Riga, A.; Alexander, K. (2014). "Solid- and liquid-state studies of a wide range of chemicals by isothermal and scanning dielectric thermal analysis." Journal of Thermal Analysis & Calorimetry, 115(3), 2253.
[62] Gardiner, D. J.; Graves, P. R. Practical Raman Spectroscopy. 1st ed. New York: Springer, 1989.
[63] Flory, P. J. Principles of Polymer Chemistry; Cornell University Press, Ithaca, 1953.
[64] Ward, I. M. Mechanical Properties of Solid Polymers; Wiley Interscience, New York, 1971.
[65] Belibel, R.; Barbaud, C.; Mora, L. (2016). "Dynamic contact angle cycling homogenizes heterogeneous surfaces." Materials Science & Engineering C, 691192-1200.
[66] Strobel, M.; Kirk, S. M.; Heinzen, L.; Mischke, E.; Lyons, C. S.; Endle, J.; Dillingham, G. (2015). "Contact angle measurements on oxidized polymer surfaces containing water-soluble species." Journal of Adhesion Science & Technology, 29(14), 1483-1507.
[67] D. Li, A.W. Neumann, in Applied Surface Thermodynamics, ed. by J.K. Spelt, A.W. Neumann (Dekker, New York, 1996), p. 109.
[68] R.V. Sedev, J.G. Petrov, A.W. Neumann, J. Colloid Interface Sci. 180, 36 (1996).